RESEARCH REPORT

External Research Program

Modelling of Road Noise and Optimal Barrier Design

Canada

CMHC SCHL

HOME TO CANADIANS

CMHC—HOME TO CANADIANS

Canada Mortgage and Housing Corporation (CMHC) has been Canada's national housing agency for more than 60 years.

Together with other housing stakeholders, we help ensure that Canada maintains one of the best housing systems in the world. We are committed to helping Canadians access a wide choice of quality, affordable homes, while making vibrant, healthy communities and cities a reality across the country.

For more information, visit our website at **www.cmhc.ca**

You can also reach us by phone at 1-800-668-2642 or by fax at 1-800-245-9274.

Outside Canada call 613-748-2003 or fax to 613-748-2016.

Canada Mortgage and Housing Corporation supports the Government of Canada policy on access to information for people with disabilities. If you wish to obtain this publication in alternative formats, call 1-800-668-2642.

MODELLING OF ROAD NOISE AND OPTIMAL BARRIER DESIGN

By K.R. Fyfe and C.C. Harrison
Department of Mechanical Engineering
4-9 Mechanical Engineering Building
University of Alberta
Edmonton, Alberta T6G 2G8

March 1995

CMHC Project Officer: Duncan Hill

This project was carried out with the assistance of a grant from Canada Mortgage and Housing Corporation under the terms of the External Research Program (CMHC CR File 6585-F039). The views expressed are those of the authors and do not represent the official views of the Corporation.

NOTE: LE RÉSUMÉ EN FRANÇAIS SUIT IMMÉDIATEMENT LE RÉSUMÉ EN ANGLAIS.

ABSTRACT

Over the past 40 years, many agencies have sought to develop predictive algorithms for computing road noise barrier performance characteristics. Typically, in order to keep the evaluation simple, these algorithms have incorporated geometrical considerations that ignore the phase information of sound waves. The intention of this report is to describe and compare traditional ray-based models with more recently developed wave-based models. A wave-based technique will then be demonstrated in a comparison of configurations with variations of the barrier's size, shape, absorptive coatings and general orientation. A rating parameter will also be introduced as the potential basis for the formulation of a set of correction factors to be applied based on the geometrical properties of the barrier configuration.

Executive Summary

Numerous models have been developed around the world for conducting road noise studies that claim to account for many geometrical factors and acoustic properties, but most, if not all, have been carried out using geometric, energy-based analysis that by in large ignore phase. This assumption is valid for higher frequency regimes, but is inadequate for the low frequency spectrum typical of traffic noise. This report describes and compares traditional energy-based models with more recently developed wave-based models. In particular, a two dimensional boundary element model is applied to systematically compare variations of the barrier's size, cross-sectional shape, absorptive coatings and general orientation. A barrier insertion loss rating parameter is introduced, that takes into account the traffic noise spectrum, to facilitate comparison of the different configurations.

Several significant relationships between barrier design characteristics and insertion loss have been observed. The results obtained for the single barrier cases suggest a basically linear relationship between the insertion loss and changes in a basic barrier parameters such as height, width, absorptive coating, as well as source and receiver locations. This suggests that results for a geometry with small variations from the standard case may be able to be tabulated, rather than recomputed for each special case.

For single barriers, absorptive coatings were found to not have significant positive improvements in the barrier performance except when the source was located close to the barrier. Alterations of the barrier cross-sectional shape were observed to have significant influence on the barrier's acoustic performance. A tee-shaped barrier, for example, was found to have an insertion loss 5dB greater than that for a semi-circular mound of the same height. Barriers on either side of the noise source have also been studied. The addition of a second barrier greatly impairs the acoustic performance of the shadow region of a single barrier unless absorptive coatings are applied to the source side of the barriers.

«Modélisation des bruits de la route et conception d'écrans optimaux»

RÉSUMÉ

De nombreux modèles ont été élaborés mondialement dans le but de mener des études sur le bruit de la circulation qui, prétend-on, tiennent compte de bon nombre de facteurs géométriques et propriétés acoustiques, mais la plupart, sinon toutes, ont été menées à l'aide d'une analyse géométrique approfondie qui ne tient pas compte de la phase. Cette hypothèse convient dans le cas d'un régime à fréquence élevée, mais pas dans le cas du spectre à basse fréquence typique du bruit de la circulation. Ce rapport décrit les modèles classiques fondés sur l'énergie et les compare aux modèles plus récents fondés sur les ondes. Particulièrement, un modèle bidimensionnel comportant des éléments de contour est appliqué pour comparer de façon systématique les variations de taille, de la coupe transversale, des revêtements absorbants et de l'orientation générale. Un indice de perte d'insertion tenant compte du spectre du bruit de la circulation facilite la comparaison des différentes configurations.

Plusieurs liens étroits entre les caractéristiques d'un écran et la perte d'insertion ont été observés. Les résultats obtenus dans le cas d'écrans simples montrent qu'il y a une relation fondalement linéaire entre la perte d'insertion et les paramètres de base tels la hauteur, la largeur, le revêtement absorbant ainsi que le type et l'emplacement du récepteur. Cela indique que les résultats obtenus pour un écran dont la forme diffère peu de l'écran standard pourraient être établis sous forme de table plutôt que de nécessiter de nouveaux calculs dans chaque cas particulier.

En ce qui a trait aux écrans simples, les revêtements absorbants n'améliorent pas de façon appréciable leur performance, sauf lorsque la source du bruit se trouve à proximité. Les modifications apportées à la forme transversale de l'écran ont, par contre, exercé une influence significative sur la performance acoustique. Par exemple, la perte d'insertion d'un écran ayant la forme d'un «t» est plus élevée (5 dB) que celle d'un talus semi-circulaire de la même hauteur. On a aussi étudié la performance d'écrans des deux côtés de la source du bruit. L'ajout d'un second écran nuit grandement à la performance acoustique de la zone d'ombre d'un écran simple à moins d'appliquer un revêtement acoustique du côté de la provenance du bruit.

National Office
700 Montreal Road
Ottawa ON K1A 0P7
Telephone: (613) 748-2000

Bureau national
700 chemin de Montréal
Ottawa ON K1A 0P7
Téléphone : (613) 748-2000

Puisqu'on prévoit une demande restreinte pour ce document de recherche, seul le résumé a été traduit.

La SCHL fera traduire le document si la demande le justifie.

Pour nous aider à déterminer si la demande justifie que ce rapport soit traduit en français, veuillez remplir la partie ci-dessous et la retourner à l'adresse suivante :

Centre canadien de documentation sur l'habitation
Société canadienne d'hypothèques et de logement
700, chemin Montréal, bureau C1-200
Ottawa (Ontario)
K1A 0P7

Titre du rapport: _____

_____

Je préférerais que ce rapport soit disponible en français.

NOM _____

ADRESSE _____
rue App.

_____
ville province Code postal

No de téléphone ( ) _____

TABLE OF CONTENTS

LIST OF FIGURES

LIST OF TABLES

1.0 INTRODUCTION

In response to public concern over road noise, numerous agencies have attempted to model roadways and traffic flows for use in developing algorithms for the prediction of surrounding noise levels. As a result of this research, several procedures for predicting and calculating noise levels have been developed. Within these models are several parameters that contribute to the overall sound level; the type of traffic, the volume and speed of traffic, source and receiver positions, ground reflectivity and absorptivity, barrier insertion loss and absorptivity, and atmospheric conditions. This report studies different methods of calculating one of these parameters, namely barrier insertion loss.

There are a large variety of techniques used to calculate road noise levels and in particular, the barrier effects on this sound level. These algorithms range from simple, hand calculations, to computer simulations, to exacting finite element techniques. This paper will examine the progression of a selection of the simple methods to the development of the more rigid, design solutions as a step to prepare for the comparison the predictive capabilities of these methods. In particular, two main classifications of these techniques will be examined. The algorithms known as the Maekawa method [1], the Kurze method [2], the Hand method [3], the Federal Highway Administration (FHWA) method [4], the Canadian Mortgage and Housing and Corporation (CMHC) method [5], the Welsh Department of Transport (Crown) method [6], the International Standards Organization (ISO) method [7] will form a group of ray tracing models. A boundary element model (BEM) [8] as well as a recently developed infinite wave envelope finite element method (FEM) [8] will be discussed as a group of wave based models.

Though much work has been conducted in the area of defining barrier performance characteristics in the presence of roadways and traffic flows, due to computational capacity constraints, one area that has not been addressed adequately is the use of these algorithms for the selection of an optimal barrier design. For any roadway, the number of potential geometrical configurations can be immense. Thus, the accurate assessment of a barrier's

performance with one of these traditional methods could require many time-intensive calculations and comparisons.

Along with an investigation of some of the shortfalls of some common currently used algorithms, this report will introduce a more effective method of calculating a barrier's performance. This method combines source strengths and receiver locations, thereby reducing the number of variable parameters, to emulate a human perception of traffic noise. This combination will permit the representation of a barrier rating with a single number. The procedure can then be used to discuss the effects of changing the barrier design. Design characteristics such as height, width, shape and absorbent coating will be considered. In addition, the application of this method will be extended to the consideration of source position, multiple barriers, and briefly, elevated and depressed roadways. Also, some general comments will be made regarding modelling limitations and alternate barrier selection criteria.

2.0 ALTERNATIVE METHODS

The distinction between ray and wave based methods should be more clearly defined. The basic difference between the ray tracing approach and the wave based procedure is in modelling the behaviour of sound. A diffraction method considers sound as a series of rays. Each ray follows a series of straight paths from the source until it reaches the receiver. The procedure then utilizes a comparison between direct and diffracted rays in evaluation of the sound field. On the other hand, a wave based method considers sound as a wave. Each direct, reflected and diffracted sound wave has an amplitude and phase, and the sound field is evaluated through interference of these waves. Each algorithm will be examined in chronological order of development, as either a ray or wave based method, and with specific attention paid to the theory used and the formulation of algorithm.

2.1 Definition of Common Geometrical Parameters

Before introducing any of the methods, Figure 1 will define the basic geometrical parameters

that will be used consistently throughout the diffraction based models.

The parameters include:

- **a** - the direct distance from the source to the top of the barrier
- **b** - the direct distance from the receiver to the top of the barrier
- **d** - the direct distance from the source to the receiver
- $\mathbf{r_o}$ - the length of the projection of 'a' in the barrier plane
- **r** - the length of the projection of 'b' in the barrier plane
- **d'** - the length of the projection of 'd' in the barrier plane
- **IL** - the barrier insertion loss
- $\boldsymbol{\theta}$ - the angle from the receiver side of the barrier to the projection of 'b'
- $\boldsymbol{\theta_o}$ - the angle from the receiver side of the barrier to the projection of 'a'

Note that $a = r_o$, $b = r$, and $d = d'$ when only two-dimensional cases are considered. These symbols will be used throughout the presentation of each method. This will serve for consistency of approach while sacrificing familiar forms of some equations.

2.2 Maekawa Method

Maekawa's method [1], developed in Japan, utilizes the Kirchoff theory of diffraction [9], which embodies most of the diffraction theory offered by Fresnel [10]. Fresnel's theory offers one explanation of diffraction around an edge. A more detailed outline of the Fresnel theory is offered in Appendix B. Maekawa paralleled this theory to sound ray diffraction and adopted two original Fresnel calculations. Through model experimentation, Maekawa developed his own formulation relating the path length difference and the Fresnel number to the barrier attenuation.

Fresnel defined the path length difference, δ, as the difference between the distance from the source to a point on a succeeding wavefront, in this case the point at the tip of the barrier, to

the receiver and the length of a direct path from the source to receiver, as in Figure 2. The path length difference was considered positive if the barrier interrupted the line of sight between the source and the receiver.

$$\delta = a + b - d$$

The Fresnel number, **N**, was then defined as the number of half wavelengths of path length difference,

$$N = \frac{2\delta}{\lambda}$$

The Maekawa algorithm was designed to calculate the shielding effect with a single graph, and without the use of computers [1]. In 1965, Maekawa proposed his attenuation chart, Figure 3, relating the Fresnel number to the attenuation. The following formulae for the semi-infinite screen describe the results on his chart.

$$IL = 20\log_{10}\frac{2\pi\sqrt{(N/2)}}{\tanh(\pi\sqrt{(N/2)})} \qquad \text{for } N < 1$$

$$IL = 10\log_{10}(20N) \qquad \text{for } N \geq 1$$

The barrier attenuation can be calculated directly from this equation or observed on the chart. Attenuation of ground reflections were computed for the receiver by repeating the procedure above for a receiver located equidistant beneath the ground as the original receiver was above the ground. The two levels were then added, with no consideration of phase [1], to obtain the barrier attenuation. Maekawa's method was later expanded to include line sources, however the formulation presented here is the one most commonly associated with a road noise application.

2.3 Kurze Method

In 1973, Kurze and Anderson [11], noting that Maekawa conducted model experiments with unconvincing geometry, chose to develop a refined method for calculation of barrier attenuation [2]. Kurze based his attenuative algorithm on the diffraction theory described by Keller [12].

Keller's geometrical theory of diffraction was based on the definition of a diffracted ray. Keller, like Fresnel, addressed the diffraction of light rays and then Kurze, in turn, paralleled the theory to sound rays. Keller explained that amplitude of a diffracted ray is determined by multiplying the incident ray by a diffraction coefficient. The coefficient decreases as the wavelength of the incident ray decreases. Therefore, the conclusion that there will be more diffraction into a shadow zone at higher wavelengths or lower frequencies. Thus, it can be expected, that at these lower frequencies, more rays will reach the shadow zone and the screen will have a less attenuative effect [13]. Keller hypothesized that diffraction was an edge effect, not explained by geometrical optics. He proceeded to develop an asymptotic solution for the attenuative effect of a semi-infinite screen. The solution for the barrier insertion loss as presented by Keller being:

$$IL = -20\log_{10}\frac{d}{4\pi\sin\beta}\left[\frac{\lambda}{ab(a+b)}\right]^{1/2}\left[\frac{1}{\cos(\theta_o-\theta)/2}+\frac{1}{\cos(\theta_o+\theta)/2}\right]$$

Kurze compared the Keller formulation to early work by Redfearn [9] and Maekawa and decided to develop a modified version. Kurze attempted to derive a formula that would correct shortcomings in the previous methods. The following is Kurze's modified version of Keller's theory.

$$IL = 10\log_{10}\left(8\pi^2\frac{h}{\lambda}\tan\psi/2\right) - 10\log_{10}\left[\frac{d^2}{d'(a+b)}\right] - 20\log_{10}\left[1+\frac{\sin\psi/2}{\sin(\theta+\psi/2)}\right]$$

The four terms in Kurze's formulation account for the Redfearn calculation [14], a correction for large path length differences, a correction for proximity of source and receiver to the screen and a factor for the angle of diffraction, respectively. This formulation, however, was still only applicable for a point source and point receiver.

2.4 Hand Method

The Hand method [3] was an approach designed to complement its associated computer program and was named for the way it was to be calculated, by hand. This method was developed by

Alberta Transportation in 1975. The method defines three sets of parameters: traffic, propagation and shielding. It is interesting to note the attempt to classify the vehicle type, volume and speed along with the roadway design in order to contribute effects to a equivalent source. This is the first method discussed that attempts to breakdown the problem into constituent parts in hopes of more appropriate modelling. At the same time, the ground and barrier attenuation effects are segregated. This is done to reduce the complex and repetitive computing of pressure levels, for each of the four propagation paths in Figure 4, should the source and receiver both be above ground level. Hence, the ground effect is not taken into account [15]. It is only the shielding parameters that are of interest here. The algorithm considers traffic as a line source. For computation, the source is assumed to be at the minimum distance from the receiver, along the roadway. The barrier length is then used to compute a subtended angle, demonstrated in Figure 5 or angle that the receiver is shielded from the road. The barrier attenuation is calculated with the following formulae, first for an infinite barrier with the otherwise identical geometry,

$$A_{180^\circ} = 15\log_{10}\left[\frac{\sqrt{20.6\delta}}{\tanh\sqrt{20.6\delta}}\right] + 5 \qquad \text{for } \delta < 5\ m$$

$$A_{180^\circ} = 20 \qquad \text{for } \delta \geq 5\ m$$

and secondly for the finite barrier,

$$IL_\theta = -10\log_{10}\left[\left(\frac{180 - \theta}{147}\right)^{1.5} + \left[1 - \left(\frac{180 - \theta}{147}\right)^{1.5}\right]10^{-A_{180}/10}\right] \qquad \text{for } \theta \geq 90^\circ$$

$$IL_\theta = -10\log_{10}\left[\left(1 - \frac{\theta}{180}\right) + \left(\frac{\theta}{180}\right)10^{-A_{180}/10}\right] \qquad \text{for } \theta < 90^\circ$$

In the development of the Hand method, the authors observed that, in a single hand calculation, the method attempts to overpredict the attenuative effect of a barrier because the single calculation can not support the precision and multiple calculation capabilities of its associated computer program.

2.5 FHWA Method

The 1978 United States Federal Highway Administration returned to the principles used by Maekawa to develop its traffic noise level prediction method. The FHWA method also uses a similar procedure to that of the Hand method. The FHWA defines one reference level and includes four adjustments [4]. A reference energy mean emission level is established and then adjustments for traffic flow, distance, finite roadway and shielding are made. Again, in this study, it is only the shielding parameter that is of interest. As did the Maekawa method, this method incorporates the path length difference and Fresnel number and then draws a relation between the Fresnel number and the insertion loss by the following set of equations.

$$\Delta_i = 0 \qquad N_i \le -0.1916 - 0.0635\epsilon$$

$$\Delta_i = 5(1 + 0.6\epsilon) + 20\log_{10}\frac{\sqrt{2\pi|N_o|_i\cos\phi}}{\tan\sqrt{2\pi|N_o|_i\cos\phi}} \qquad (-0.1916 - 0.0635\epsilon) \le N_i \le 0$$

$$\Delta_i = 5(1 + 0.6\epsilon) + 20\log_{10}\frac{\sqrt{2\pi(N_o)_i\cos\phi}}{\tanh\sqrt{2\pi(N_o)_i\cos\phi}} \qquad 0 \le N_i \le 5.03$$

$$\Delta_i = 20(1 + 0.15\epsilon) \qquad N_i \ge 5.03$$

$$IL = 10\log_{10}\frac{1}{\Delta\phi}\int_{\phi_L}^{\phi_R} 10^{-\frac{\Delta_i}{10}}\, d\phi$$

The line source is represented by a collection of moving point sources considered to be centered at an average distance from the barrier. In the attenuation calculation, the barrier length is accounted for by integration over the subtended angles, now redefined in Figure 6, to either side of a perpendicular from the receiver through the barrier. The FHWA assessed its own accuracy through comparison with a limited number of field measurements. The FHWA appears as one of the most widely accepted methods, in North America, for prediction of traffic noise levels.

2.6 CMHC Method

The CMHC method [5] was developed in 1980 by research supported by the Canadian Mortgage and Housing Corporation. The CMHC method uses a similar association between the geometrical parameters and the barrier attenuation. However, instead of formula, reference tables (Appendix C) are provided for evaluation of the insertion loss. The first table, Table C1, determines an effective barrier length ratio, $\mathbf{l}_{\mathbf{eff}}$, derived from the relations of the receiver distance from the barrier and the length of the barrier associated with Figure 7.

$$l_{eff_l} = u/g$$
$$l_{eff_r} = v/g$$

Next, the path length difference,

$$\delta = a + b - d$$

the effective barrier length ratio and the interruption of line of sight between the source to the receiver are combined in Table C2 to yield the insertion loss. The CMHC method abandons the Maekawa declaration that the path length difference can be positive or negative. In this algorithm, the path length difference is considered positive with a location in either of the shadow or illuminated zones. The CMHC method is frequency independent. A line source is considered in the evaluation by placing a source at the midline of the roadway and intersecting with a path through the receiver and perpendicular to the barrier and roadway.

For more complex geometries, such as roadway depressions and changes in ground elevation, a parameter called the total effective height is introduced. This effective height, h_{eff}, is evaluated as the sum of the source height above ground, the receiver height above ground, twice the barrier height and any change in ground elevation.

$$h_{eff} = s + r + 2h_b + e$$

Then, the effective height is matched against the horizontal distance between the source and receiver to obtain a distance correction factor from Table C3. This distance correction factor is then added to the barrier attenuation in the overall sound level.

2.7 Crown Method

In 1988, a method was developed under the Department of Transport, Welsh Office, and will herein be referred to as the Crown method [6]. It introduced a frequency dependent way of calculating the attenuative effects of a barrier. As in the CHMC method, the Crown method reduces a line source by replacing it with an effective point source located at the midpoint of the source line. With this effective point source, the path length difference, δ, can be calculated as in previous methods. A parameter, **x**, based on the path length difference, was then established for use in the algorithm,

$$x = \log_{10}\delta$$

By compiling results from previous research, relations to this parameter and the barrier attenuation could be investigated. Fifth and seventh order polynomial regressions were used to approximate this relation.

$$A = A_0 + A_1x + A_2x^2 + \ldots + A_nx^n$$

Then, dependant on whether the receiver lies in the shadow or illuminated zone, different coefficients are applied to $\mathbf{A_0}$, $\mathbf{A_1}$, $\mathbf{A_2}$, ...$\mathbf{A_n}$. and the attenuation can then be calculated with the appropriate formula, using Tables D1 and D2 (Appendix D), in the specified range of validity.

2.8 ISO Method

In 1992, The International Standard Organization offered a general method of calculation of attenuation of sound during propagation outdoors [7]. The procedure attempts to discuss various

sound sources, including road traffic. The ISO defines a line source as a group of point sources. Furthermore, a group of point sources can be approximated by an equivalent, single point source in the centre of the group should the sources have "approximately the same strength and height above the local ground plane, the same propagation conditions to the point of reception, and the distance from the equivalent source to the receiver exceeds twice the largest diameter of the relevant area of sources" [7]. Otherwise, the line source must be computed segment by segment. Though the algorithm is frequency dependent, there is suggestion of considering the attenuation at 500 Hz to be representative of the entire range of traffic emissions [7]. The insertion loss of a barrier can be represented by the following expression.

$$IL = D_z - A_{ground}$$

The two terms represent a screening index,

$$D_z = 10 \log_{10}(3 + (C_2/\lambda) C_3 \delta K_w)$$

where the constants $C_2 = 20$ includes effects of ground reflections, $C_3 = 1$ for single diffraction (thin screen) and $\mathbf{K_w}$, the meteorological correction factor, can be computed as follows,

$$K_w = e^{-\frac{1}{2000}\sqrt{\frac{abd}{2\delta}}} \quad \text{for } \delta > 0$$
$$K_w = 1 \quad \text{for } \delta \leq 0$$

and a ground effect,

$$A_{ground} = 4.8 - (2\frac{h_m}{d})(17 + \frac{300}{d})$$

with $\mathbf{h_m}$ being the mean height of propagation. A negative value for the ground term shall be replaced by a zero. For most of the cases considered here, where d is less than 20m, this term will be zero, and thus, the screening index is the only component of the attenuative term.

2.9 Boundary Element Method

The boundary element method [8,16,17], a numerical analysis approach, derives an integral solution to the Helmholtz acoustic wave equation. The Helmholtz equation:

$$\nabla^2 p + k^2 p = 0$$

describes the sound field produced by a radiating vibrating surface where **p** depicts the acoustic pressure and **k** is the wave number (ω/c). To solve the differential equation, fixed pressure or fixed velocity boundary conditions, or normal or transfer impedance boundary conditions must be applied to the surface of the emanating body. The boundary element method can be developed by applying Green's Theorem to the Helmholtz integral equation. A direct approach solves for the acoustic pressure or acoustic velocity. For an exterior problem, the Helmholtz integral equation is as follows:

$$p(X) = \int_S \left[p(Y) \frac{\partial G(X,Y)}{\partial v} - G(X,Y) \frac{\partial p(Y)}{\partial v} \right] dS(Y)$$

where X and Y are the receiver and source positions, respectively. For the two dimensional geometries to be considered in this study, Green's function has the form,

$$G(X,Y) = \frac{j}{4} H_0^{(1)}(kR)$$

where $\mathbf{H_0^{(1)}}$ is the Hankel function of the first kind and order zero and where **R** is the distance between the source and receiving points. A model of nodes, spaced six per wavelength, and connecting elements is developed to define the surface geometry. Applying the Helmholtz integral equation to each node in the calculation mesh results in a system of equations of the form:

$$[A(\omega)]\{p\} = [B(\omega)]\{v\}$$

The boundary conditions described above are then applied. The field point pressures, or other

acoustic variables, can then be evaluated by solving the system. The field point pressures can be manipulated, through further calculation, to yield the insertion losses associated with each field point.

2.10 Finite Element Method

The finite element method [8,18,19] approaches the solution to an exterior radiating acoustic problem with a Galerkin residual or variational procedure for evaluation of the Helmholtz equation. The field can be divided into small subregions, known as finite elements. The elements connect a grid of nodes spaced traditionally six every wavelength. The acoustic pressure can then be determined, anywhere within one of these elements, with an appropriate shape function N, either a linear or quadratic function.

$$p = [N_1 \cdots N_m] \begin{Bmatrix} p_{e_1} \\ \vdots \\ p_{e_m} \end{Bmatrix} = [N]\,[p_e]^T$$

Elemental mass $[M_e]$ and stiffness $[K_e]$ matrices can be combined to form global matrices and form the equation:

$$([K] - \omega^2 [M])\{p\} = \{f\}$$

for the evaluation of a forced response. The evaluation can again be manipulated such that results are presented in terms of insertion loss rather than field pressure.

As it is impossible to model an infinite domain with a finite number of elements, the finite element method must model a significantly large enough plane such that arbitrary boundary conditions applied at the edge of the plane do not affect the conditions close to the source and receiver. Doing this requires the application of large numbers of boundary conditions and the computation for large numbers of nodes. To reduce the need for such a large number of conventional elements, and in turn, reduce the computational time required for such a model, an improved finite element, an infinite wave envelope (WE) element [20] can be implemented

as an alternate means of modelling infinite planes.

An infinite WE element is attached to the conventional finite element mesh and stretches to infinity. The infinite WE involves finite to infinite geometry mapping of the parent element, the addition of acoustic nodes between the geometrical nodes in a given element, the use of Lagrangian polynomials as a special shape function, and the use of the complex conjugate of these shape functions as a weighting function. These changes will still permit the use of the finite element procedure described above.

2.11 Commercial Programs

There are numerous computer programs available commercially or through their respective creators. These methods will not be evaluated because they are variations of the approaches described and because it is difficult to modify the code within each program to isolate the barrier contribution to the overall sound level. Computer traffic models include:

BRUIT (France),
MODEL 77 (Switzerland),
MWAY (United Kingdom) [14],
ORNAMENT/STAMSON (Ontario) [21],
BAROP, ROBARD, SOUNDPLAN, CROSECT (Britain) [22],
STAMINA/OPTIMA [23], IMAGE-3 (United States) [24].

3.0 COMPARISON OF ALTERNATIVE METHODS

This section will outline some necessary assumptions in order to make the methods described compatible and comparable. After defining the barrier insertion loss as the performance measure, some preliminary tests are conducted to compare ray and wave based procedures.

3.1 Underlying Assumptions

Ideally, it would be most suitable to model a roadway in three dimensions, where constructions such as corners, overpasses and changes in number of lanes, barrier height and ground cover could be accommodated. Many of the methods chosen for comparison are incapable of handling the mathematical complexity of such a geometry. Therefore, it is necessary to simplify the scheme and consider only a two dimensional model. Cross sections of the traffic flow, roadway and barrier will be considered. As each algorithm accounts for different constraints in different manners, it is necessary to reduce the model to a basic geometry so that they can become comparable. As a consequence, the following assumptions are made in the modelling:

(1) A stream of traffic can be considered as a line source represented by a series of point sources, a cylindrical source or an equivalent point source.

(2) The roadway and barrier are parallel and of infinite length and of constant width and height.

(3) The source and receiver plane is perpendicular to both the roadway and the barrier.

(4) The barrier construction material is dense enough (20 kg/m^2) such that the transmission loss through the barrier is negligible in comparison to the insertion loss provided by the barrier [14].

(5) The entire ground is perfectly reflecting, representing hard ground or asphalt cover.

(6) The source and receiver positions are considered stationary, thus eliminating any Doppler effects.

(7) The density of air is 1.225 kg/m^3 and the temperature of air is such that the speed of

sound, c, will be 340 m/s. There are no other extremities in atmospheric conditions that would adversely affect sound propagation.

(8) A frequency range up to and inclusive of 4000 Hertz will be assessed.

In order to make a consistent comparison of the predictive algorithms, a standard for comparison must be established. It is suggested that a barriers' performance will be evaluated in terms of insertion loss, measured in decibels (dB). The insertion loss can be defined as the reduction in sound level observed after the barrier has been placed in the field in comparison to the sound level of the identical field with no such barrier. It is common, however, that performance of a barrier is assessed in terms of barrier, or excess, attenuation. Barrier attenuation can be defined as the difference between the barrier field sound level and the free field sound level. However, it is revealed that, for perfectly reflecting ground [3], combined with a source located on the ground [25], barrier attenuation and insertion loss are equivalent.

3.2 Implementation and Applications

The algorithms for the ray tracing methods were programmed in such a manner that the insertion loss could be calculated for simple two-dimensional geometries, according to the assumptions previously made. The programs were a direct application of the methods discussed herein and in earlier work [26]. A model geometry was defined by erecting a barrier, of chosen height, at the origin and specifying source and receiver coordinates in front of and behind the barrier, respectively.

The boundary element method (BEM) modelling and calculation occurred in three stages. The boundary surface was defined utilizing a finite element pre-processor. Using the ANSYS 5.0 [27] finite element package, an input mesh was created by outlining the surface boundary using nodes, discretized at six nodes per wavelength, and connecting adjacent nodes with conventional linear elements. The pre-processor thus served to define the barrier and ground layout geometry. A sample mesh is provided in Figure 8. The mesh depicts two barriers on a flat

ground plane. This mesh was then read into the SYSNOISE (System for Numerical Noise Analysis) [28] software package. Here the source position and frequency as well as the receiver position was defined. SYSNOISE then calculated the field point pressures at desired locations. The final stage in the BEM analysis involved using ANSYS as a post-processor to display the resulting pressure field. Thus, ANSYS was used as a visual aid in modelling and observing results, whereas SYSNOISE was responsible for the mathematical computation.

Similarly, the finite element method (FEM) used ANSYS to define a mesh to model the acoustic field. Conventional quadratic elements and ninth order infinite wave envelope elements [20,29] were used in the model. Figure 9 illustrates the FEM mesh for the same geometry as used for the sample BEM mesh. However, to process this field, a computer program entitled Wave2D [29] was used. Either ANSYS or the Wave2D package could be used to display contours of the field point pressures. For both the BEM and FEM, small programs were written to convert the field point pressures of the calculated and free fields to the insertion loss.

3.3 A Sample Comparison

The geometry considered was that of Hothersall et al. [25] with a source located on the ground, 15m behind a 3m tall barrier and with a receiver located on the ground and 50m behind the barrier. Figure 10 depicts this geometry. The results of the nine methods (seven ray based and two wave based) were compared with the results of Hothersall et al. [25]. Figure 11 shows the nine sets of results for insertion loss frequency sweeps of this geometry while, for comparison, the Hothersall et al. findings are provided in Figure 12, on the curve labelled 3m.

The comparison between these two charts yields some trends and some immediate dissimilarities. Firstly, the CMHC, the Hand and the Crown method are frequency insensitive, thus accounting for the straight lines in the graph. It is clear, however, by observing the other results, that there is an obvious dependence of insertion loss on frequency.

The next noticeable claim is that the Maekawa, FHWA and ISO curves are situated very close

to or on top of each other. This is an observed, but well predictable, trend and stems from the consistent use of Fresnel theory for path length difference. These three methods also estimate the Hothersall et al. results within 2 dB.

Following a moderately different slope is the Kurze and Anderson curve, depicting an insertion loss of approximately 3-4 dB greater than any other method. The Kurze method shows slightly different results due to its basis on the Keller theory of diffraction and the use of a point source versus a line source.

The BEM and FEM results most closely approximate those of Hothersall et al., varying by 1 dB through the 1000 Hz range. The FEM curve strays from the BEM curve above 200 Hz. The FEM results above 200 Hz are invalid as the model deteriorates beyond this frequency, and results of this method are not presented beyond 200 Hz. A greater limiting frequency for the FEM could be achieved by spending considerable time on the rigorous modelling of smaller elements required at high frequencies. It will be suggested then, that because of an observed maximum difference of 0.5 dB between the BEM and FEM in a frequency range where both models are valid, that refinements to the FEM modelling capabilities will yield identical results to those of the BEM at higher frequencies currently outside the FEM range of validity. Thus, the two techniques, based on different theory, would yield virtually the same results.

One final note, with the exception of the Kurze formulation, another interesting characteristic of Figure 11 is the convergence, within 3 dB, of the diffraction based models in the 400-650 Hz range. This supports the Hand, CMHC and Crown methods' claims that perhaps a broadband of traffic frequencies can be represented solely at one frequency, 500 Hz. It is thought that the 500 Hz results are representative of the entire range of traffic emissions [7]. While many observers agree that the energy emissions in a traffic spectrum are greatest near 500 Hz [5,7], these ray-based procedures ignore the remaining frequency content of the traffic spectrum.

The objective of this preliminary examination was to compare ray tracing and wave-based road noise prediction techniques in terms of calculating the attenuative effect of a barrier. A primary

difference between the two types of procedures is the complexity of geometrical problems that can be evaluated. The diffraction based methods offer a quick, simple reference for the prediction of insertion loss in basic geometrical situations. While a wave-based model provides accurate results by correcting the ray-based methods neglect of interference effects, it does so at the expense of larger models and increased computational time. For this reason, many studies [25,30] have examined barrier performance at a single source and single receiver position. The calculational accuracy of these methods has not yet been put to rigorous test and instead, generalizations about the overall barrier performance have been made based on a single geometry or small samples of geometries.

Hothersall et al. [25] have studied the average insertion loss at five receiver points in order to make relative comparisons between barriers. However, the chosen receiver locations don't necessarily provide an adequate representation of the affected field. In addition, the use of a wave-based model permits calculations at discrete frequencies. This allows the implementation of a broadband source covering the entire traffic spectrum. The Hothersall study shows significant discrepancies between broadband and 500 Hz source results, affirming the notion that an analysis solely at 500 Hz may not be adequate. It is in the presence of these shortfalls in the ray-based methods that this report proposes a new method to rate the overall performance of a sound barrier.

4.0 CONSTRUCTION OF BARRIER RATING SYSTEM

The challenge in designing a system for road noise barrier rating is how to manipulate the use of source frequency, amplitude and position and receiver position into these discrete analysis modelling tools such that the results are indicative of realistic traffic scenarios. We will first consider how to represent an entire traffic flow with a single point source. The frequency response of traffic noise has been measured by several researchers [31,32]. In Figure 13, curve A shows Lyon's [32] measurement of the frequency content of traffic noise. It is apparent that the majority of the energy is concentrated in the range below 1000 Hz. This is the acoustic pressure that would be recorded by a microphone with a uniform frequency response. But,

because the human ear is most sensitive to sound in the 1000 to 4000 Hz range, this curve does not show the human perception of traffic noise. By including the A-weighting curve [33], shown as curve B in Figure 13, the traffic noise spectrum can be altered to represent the human perception of traffic noise. There is no difficulty in applying this A-weighting to the source, rather than the receiver, as the effect of weighting the sound level at the source or receiver position is the same.

The result of combining these two curves is an A-weighted traffic noise spectrum, as demonstrated by curve C in Figure 13. Despite the higher sound level at low frequencies, the human ear can not recognize this sound. Similarly, although the human ear is sensitive at higher frequencies, traffic does not emit as much sound energy at these higher levels. Hence, the inverted U-shaped spectrum. Here it can be seen that the concentration of the energy near 500 Hz suggests the use of this frequency as a basis for the ray-based models. The proposed technique, however, will use the distribution of the energy in this spectrum to weight the amplitude of the source at discrete frequencies.

One way to represent a broadband source is by combining results at one-third octave centre frequencies or at octave center frequencies. It will be shown later that, applying this new system to a simple configuration, the results at the seven octave frequencies between 62.5 and 4000 Hz will yield virtually the same results as the 25 one-third octave frequencies between 15.625 and 4000 Hz. The distribution of the energy in this spectrum can now be used to weight the amplitude of the source using the following formula:

$$p_i^2 = 10^{\frac{dB}{10}} * p_{ref}^2$$

$$w_{energy_i} = \frac{\frac{p_i^2}{p_{500}^2}}{\sum_{n=1}^{\infty} \frac{p_n^2}{p_{500}^2}}$$

where $\mathbf{p}_i^2$ is the energy at frequency i based on the decibel level obtained from the A-weighted traffic noise spectrum. The pressure weight can then be determined as the square root of the

energy weight. Table 1 summarizes these weights for the seven discrete frequencies between 62.5 and 4000 Hz.

Then, to achieve an equivalent source amplitude of one, the field point energy levels (ie. $\mathbf{p}^2$ values) at the discrete frequencies need only to be added together.

The last step in the procedure consists of reducing this "frequency-averaged" result at each location into a single parameter. This single parameter then would represent the average performance of the barrier across the receiver field of interest. For this study, the arithmetic mean of the frequency averaged insertion losses at each location is taken as the single performance rating of the barrier. An example of this procedure will be shown in the following section.

Table 1 - Traffic Spectrum Energy and Pressure Weights

Frequency	Energy Weight	Pressure Weight
62.5	0.003	0.051
125	0.037	0.193
250	0.199	0.446
500	0.414	0.643
1000	0.305	0.553
2000	0.040	0.201
4000	0.002	0.043

In order to be consistent, barrier performance will be measured in terms of insertion loss throughout this paper. Recall that the insertion loss is defined as the difference between the free field and barrier field sound levels. One advantage to using insertion loss over another performance measure is that a barrier will produce the same insertion loss despite the initial strength of the source. Therefore, it is not critical to evaluate the exact initial strength of the source.

5.0 THE STANDARD GEOMETRY

The benchmark case for the following analyses will be that of a geometry consisting of a source position of 15m in front of the center of the barrier, 0.5m above ground with 20 receiver locations spaced every 5m behind the barrier at a height of 1.5m. The source height was chosen as the average height of a vehicle motor and the receiver height was chosen as the average height of a human ear. The standard barrier will be a straight, hard barrier 3m in height. Figure 14 depicts this geometry. All barrier configurations considered will be variations of the characteristic dimensions presented in the standard case. This geometry will be used to demonstrate the proposed barrier rating system procedure.

6.0 DEMONSTRATION OF THE TECHNIQUE

Implementing, now and for all further experimentation, the boudary element technique, the insertion loss curves at octave center frequencies for this simple hard thin barrier as a function of receiver distance from the barrier are shown in Figure 15. It can be seen that at any given distance, depending on the frequency of the source, the barrier rating can vary anywhere from 5 to 40 dB's of insertion loss. This emphasizes the difficulty is designing a barrier for multiple geometrical considerations. In another dimension, Figure 16 provides the insertion loss curves for specific receiver locations as a function of frequency. Again, it is easy to discern the variation of insertion loss at any frequency. To further elaborate on this point, Figure 17 depicts the insertion loss as a function of both frequency and receiver distance from the barrier. Any one position on this surface could represent the barrier performance.

By performing calculations at one-third octave frequencies and applying the A-weighted filter and corresponding energy weights, the problem can be reduced to a single value for each given distance. This frequency averaged result is shown in Figure 18. Similarly, the frequency-averaged result can be obtained for the octave center frequencies and the octave center frequencies, excluding 4000 Hz (because the sound level is very small and so is its weight). These resultant curves are also shown in Figure 18. The 500 Hz, the CMHC and the FHWA

results are shown for comparison. Even in the most basic of barrier designs, this clearly demonstrates that the consideration of the problem at only one frequency is inappropriate.

Now, we would like to take the results at each receiver location and combine them to obtain the single performance measure for the entire standard configuration. The average of the IL at each location is taken as a simple mean and the resultant parameter is an insertion loss of 11.0 dB. This suggests that the single measure for the standard case is a performance of 11.0 dB. Essentially, this has reduced a two-dimensional field of results into a single scalar value and will make different barrier configuration comparisons possible. As such, this analysis will now be extended into different basic and more complex geometries.

7.0 ANALYSIS OF BASIC GEOMETRIES

7.1 Height of Straight Barrier

The height of the barrier will be the first variation of the standard geometry to be explored. The insertion losses of barrier heights between 2m and 4m tall are shown in Figure 19. A consistent pattern emerges whereby, despite the receiver location, for each 1m increase in barrier height, an additional 2.5dB of insertion loss can be obtained. It would be expected that as the height increases, the incremental gain in insertion loss will decline. This can be expected as the insertion loss will gradually approach the limit for the maximum attenuation, i.e. that of the free field sound level. However, this trend does not appear in the practical range of barrier design heights.

7.2 Width of Straight Barrier

The sensitivity insertion loss to barrier width is also examined. A thickness range of 0.1m to 0.5m was considered. Figure 20 depicts how the insertion loss for a 3m tall straight barrier varies with the width of the barrier and the receiver distance behind the barrier. The same trend exists that there is a constant improvement in insertion loss over the range of receiver locations.

However, in this case it becomes more obvious that beyond a thickness of 0.5m there is minimal attenuative value left to be obtained by increasing the thickness. In fact, there is not even a 0.5 dB advantage from increasing the width by a factor of five from 0.1m to 0.5m.

7.3 Receiver Position

For a starting point in the analysis, 1.5m was used as an average human ear height. Because of this, the analysis has considered only one receiver height. To test the sensitivity of insertion loss to the receiver height, it was interesting to investigate the effects of changing the receiver height.

Figure 21 depicts insertion loss curves for receiver heights at 0.5m intervals between 0.5m and 2m above the ground. Two distinct regions can be observed. In the shadow region immediately behind the barrier, better attenuation is observed when the receiver is located close to the ground. Beyond 15m from the barrier and outside the shadow region, better attenuation is observed at higher receiver locations. This occurs because ground reflection have less influence on the overall sound level farther from the barrier. Near 20m, approximately 1 dB of insertion loss can be achieved for each 0.5m above the ground. However, this difference decays with distance from the barriers. In fact, this result should be expected because at large distances, it should be difficult to distinguish between two locations 0.5m apart.

7.4 Absorptive Coatings

In many applications, the material of which the barrier is constructed can have a significant influence on the performance of the barrier. In other cases, special linings are applied to the barrier surface with the specific intent of reducing sound propagation. In order to model this type of absorptive barrier with wave based models, a normal complex impedance must be applied to the boundary of interest [28]. There are several methods for rating the absorptive capacity of a material and these are described and interrelated in Appendix E. In all cases herein, unless listed otherwise, the absorptive coating will be applied only to the source side of

the barrier.

The performance of the standard barrier with an absorptive coating varying from the perfectly hard case (infinite MKS units) to a case close to perfect absorption (50,000 MKS units) is illustrated in Figure 22. It is shown that the improvement in performance is proportional to the level of absorption of the material. By incorporating the most absorptive material into the design, a 1 dB improvement in insertion loss can be observed. Though it does not appear as the absorptive coating significantly enhances the barrier performance, it will be demonstrated in the next section that the effect of absorption is greatly improved when the barrier is closer to the source.

Applying an absorptive coating to the receiver side of the barrier is redundant, at least in the case of the standard geometry, as no sound waves are ever actually directed towards this surface. In other words, the barrier would perform identically to that with just the coating applied to the source side. This is an oversimplification because as soon as any building is placed on the receiver side, this generalization would not hold.

Combining now the effects of barrier height with absorptive coatings, Figure 23 illustrates the insertion loss as a function of height for a barrier with a theoretically perfect absorptive coating and for a barrier without such a coating. These curves demonstrate that despite the height of the barrier, a 0.5 dB improvement in insertion loss can be obtained with an absorptive lining. Also, the same linear relationship that for each 1m of barrier height added, 2.5 dB of insertion loss are realized. This relationship holds for both the hard and absorptive barriers.

7.5 Source Position

Having studied the effects of varying the receiver position, it is logical to proceed with an analysis of the source position. It is important to study this effect as the vehicle represented by the source could be in different lanes of traffic and hence, farther from the barrier. Maintaining the source height of 0.5m above the ground, the source was moved between 2.5m

and 20m from the barrier. Figure 24 shows the results of this geometrical consideration.

The chart shows that the insertion loss increases dramatically as the source is moved closer to the barrier. This phenomena can be explained by the fact that as the source approaches the barrier, a greater percentage of the sound is reflected back towards the source and a lesser percentage diffracts around the top. This percentage can be related to the angle from the source to the top of the barrier. This parameter is one that is widely used in ray-based models. Similarly, the farther the source is away from the barrier, the less attenuative effect the barrier has. Beyond 50m, a 5m difference in source position has no noticeable effect on insertion loss.

Figure 25 includes the results of the identical barrier but now with an absorptive coating, in addition to those results just described. It can be seen again that as the source moves closer to the barrier, the effect of the absorption on the insertion loss increases. At a distance of 2.5m from the barrier, the absorptive coating provides an additional 3 dB of insertion loss while at a source distance of 20m, the absorption increases the performance above the standard case by only 0.5 dB. Figure 26 summarizes this relationship more clearly by displaying the insertion loss as a function of source position. This would suggest that the use of absorptive coatings is most practical when the barrier can be located very close to the roadway. This is very useful for applications with rail transportation where the construction of barriers quite close to the tracks is potentially safer.

7.6 Different Shaped Barriers

Introducing some geometrical complexity, the barrier rating system is applied to the angular, circular and T-shaped barrier designs presented in Figure 27. Each barrier has the characteristic dimension of 3m in height. Table 2 displays the combined (i.e. frequency and spatially averaged) insertion loss rating of each barrier and a rating relative to the straight barrier.

Table 2 - Combined Insertion Loss Ratings

Barrier Shape	Combined I.L. (dBA)	Relative I.L. (dBA)
T-Shaped	12.92	+1.92
Straight	11.00	0.0
Circular	9.62	-1.38
Angular	8.42	-2.58

The order of performance from most effective to least effective is as follows: T-shaped, straight, circular and angular. This order is the same as recommended by Hothersall et al. [34]. It can also be seen in Figure 28 and in all previous cases, that each insertion loss curve was essentially parallel at a far enough distance away from the barrier. This suggests that, at any distance, the relative insertion losses will be the same. Therefore, for a simple comparison of two barriers, an analysis with only one receiver location may suffice, but in the comparison of multiple shapes and sizes, it remains best to average a field of results.

7.7 Source Position and Shapes

Returning now to the analysis concerning the source position, it is interesting to investigate the effect of the source position in front of these alternate shape barriers. Figures 29 through 31 indicate that the same decaying incremental insertion loss with source position trend is evident for the angular, circular and T-shaped barriers as was for the standard barrier. Again, the barrier performs best when it is closest to the source. Combining these results to show insertion loss as a function of source position, Figure 32 can be obtained. From this figure, the angular and straight barrier performances appear to decay at a slower rate than do the circular and T-shaped barrier.

Based on the results obtained so far, there is suggestion that there may be potential for the creation of tables of correction factors to be applied to the IL of the standard barrier

configuration. A separate correction factor for the barrier shape could be constructed similar to that of the relative IL characteristic in Table 2 and then a function could be provided to evaluate the IL as it decays with source distance from the barrier.

7.8 Variations of the T-Shaped Barrier

It can be expected that for any given shaped barrier, the performance can be expected to increase with an increase in height, width or the addition of an absorptive coating. But, because the T-shaped barrier was determined to be the highest rated standard barrier, perhaps a closer look may be of interest. It becomes readily apparent that the T-shaped barrier has more geometrical parameters that could potentially be designed to further enhance its performance.

As previously discussed, by increasing the height of the barrier the performance will increase. Figure 33 confirms this once again for the T-shaped barrier. The barrier performs at about an additional 2.5 dB of insertion loss for each 1m of additional height. This is approximately the same incremental performance as for the straight barrier.

The second main dimension of the T-shaped barrier is the length of the top portion of the tee. By varying this length from zero to 2.5m, the results in Figure 34 can be constructed. The T-shaped barrier with a 0m top is in essence a straight barrier. Each 0.5m extension across the top provides approximately 0.5dB of additional insertion loss. As the top extends to a much larger distance, the tee essentially forms, with the ground, a three sided box around the source. Therefore, in theory, if the tee is extended enough, the source can be completely isolated from the receiver and thus perfect attenuation. However, this is both impractical and holds only as long as the barrier is infinitely long. In accordance with symmetry, this same box is formed on the receiver side and the shadow region is extended.

Consider now one additional case whereby an absorptive coating is applied to the top of the horizontal portion of the tee and the height of the T-shaped barrier is varied. Figure 35 depicts the insertion loss as a function of barrier height for the hard top and the absorptive top. What

can be observed is that an extra 2.5 dB of insertion loss can be achieved by applying the coating. Also, this additional 2.5 dB declines, but very slowly, as the barrier height is increased. This should be expected because as the barrier gets quite tall, it starts to resemble a straight barrier and the beneficial effects of the horizontal piece become smaller.

7.9 Parallel Barriers vs Single Barriers

In many roadway situations, it is of interest to shield both sides of the roadway from the traffic noise. As such, a single barrier will only serve to protect one side of the roadway, while at the same time increasing the sound level on the opposite side by means of sound wave reflection. To remedy this situation, the construction of a second barrier is necessary. This section studies the effect of the addition of this second barrier on the opposite side of the source from the original barrier.

Consider the case with two 3m high straight barriers 30m apart. The source remains 15m behind the original barrier and 0.5m above the ground shown in Figure 36. By making the system symmetrical, identical attenuation will be achieved behind each barrier. Figure 37 shows the insertion loss as a function of both distance and frequency. Compared to the same curve for a single barrier, Figure 17, there remains the same pattern with respect to distance but not with respect to frequency. These fluctuations from the single barrier case are present because of the multiple reflections back and forth between the two barriers.

In particular, the following single and double barrier scenarios were analyzed.

- Single Barrier
- Single Barrier with Perfectly Absorbent Coating
- Parallel Barriers
- Parallel Barriers both with Perfectly Absorbent Coating
- Parallel Barriers with 1 of 2 Barriers Coated

Figure 38 shows the insertion loss against receiver distance curves for these six cases. The most striking result is that the parallel barrier case with no impedance has the lowest performance rating. Some of the sound that was reflected by the initial single barrier is now being reflected back. The scenarios with a perfectly absorbing single barrier, and parallel barriers with a coating on the non-original barrier have identical insertion loss curves. (ie. the additional barrier absorbs all sound waves and essentially acts as if there is, in fact, no barrier). Using the same reasoning, the single barrier case with absorbent coating is equivalent to the parallel barrier case with absorbent coating. What these results suggest then is that to achieve the same performance on both sides of the road as originally intended for just one side with a single barrier, absorbent coatings are critical. In fact, an absorption coefficient of approximately $\alpha = 0.9$ is a required to restore the insertion loss of the double barriers to that of the original single barrier.

8.0 ANALYSIS OF MORE COMPLEX GEOMETRIES

Due to some of the modelling constraints that will be described later, investigation of larger and more complex geometries to this point has been limited. In order to get a basic understanding of the sound field, initial analyses were performed only at 500 Hertz. Sound pressure level contour plots are provided to illustrate both the type of geometries to be explored and the interference effects in the sound field created by these geometries.

Six main configurations are presented. These constitute a flat, depressed and elevated roadway, all with and without parallel barriers. The barriers are 5m high and spaced 25m apart. Both a car and a truck are located on the roadway. The car source is located 0.5m above the ground. The truck source is located 0.7m above the ground and has an amplitude 1.3 times the amplitude of the car. Figures 39 through 44 show the field contour plots for these geometries. Perhaps the only significant result that can be observed from these plots is that the addition of the parallel barrier provides attenuation to a large region behind the barriers. As is seen in these figures, the use of multiple barriers is an effective way of trapping sound in between the barriers and reflecting it upwards, rather than outwards.

9.0 MODELLING LIMITATIONS

Though many different configurations have been investigated, there are a great many interesting problems that are restricted by some modelling limitations. Current computational capacity limits problem meshes to a maximum of 1500 nodes for reasonable run times. Based on the need for six nodes per wavelength on the boundary, to solve full scale problems at high frequency mandates that only small boundaries can be considered. In particular, this has most greatly impeded the investigation of ground cover effects on barrier performance. In this case, the ground must become part of the boundary and to extend the boundary to any significant region of interest requires far more nodes than can currently be implemented. Also, computer time can also be expensive, particularly if investigating large fields. If such is the case, variational methods may become more affordable than the presently used collocation methods [28].

10.0 DISCUSSION

Several significant relationships between barrier design characteristics and insertion loss have be observed. The results obtained for the single barrier cases suggest a linear relationship between changes in insertion loss and changes in a basic barrier parameters such as height, width, absorptive coating, as well as source and receiver location. This suggests that results for a geometry with small variations from the standard case may be able to be tabulated, rather than recomputed for each special case.

Suppose, for example, that one wishes to investigate the performance of a 4m tall barrier with a perfectly absorptive coating with all other geometrical considerations as in the standard case. Based on the trends found herein and the performance rating of 11.0 dB for the hard 3m barrier, 2.5 dB can be added for the additional 1m of height and 1.0 dB could be added for the absorptive coating, for a total of 14.5 dB. Conducting a thorough analysis for the same case would yield a performance measure of 14.6 dB. Similarly, there could be correction factors for source position, receiver position, shape of barrier, number of barriers, etc. This set of

relationships and correction factors could potentially form the basis of a wave-based reference system for predicting barrier performance.

The results presented here logically seem to indicate that the highest, thickest, most absorptive barrier is the optimal barrier. While this is an expected result there are many considerations besides performance that relate to the community acceptance of a road noise barrier. As the construction of these barriers is generally funded by municipal and provincial governments (i.e. the taxpayers), cost control is a strict concern. In this analysis, if the cost of the barrier can be related to its cross-sectional area, approximately $16.63 US [35] per cubic foot, then the most affordable design becomes the smallest barrier. If constructing a new barrier, agencies should select an absorptive barrier. With international markets, bids for the construction of an absorptive barriers with an absorption coefficient of 0.95 are cost-competitive, if not equivalent to bids for construction of a solely concrete barrier. If, however, performance enhancement of an existing concrete barrier is of interest, design modifications such as increased height and T-shapes are more affordable [36]. Note again though that the costs are highly dependent on the particular barrier and envrionment being developed.

Other extraneous issues that should be considered are the aesthetics (color, shape, obstruction of view, human perception, etc.) of the barrier. In fact, natural barriers such as trees and bushes may be more plausible dependant upon the desired attenuation. Ideally, all of these variables have to be considered as social driving forces in the selection of a barrier design.

11.0 FUTURE RESEARCH

There exists two main directions in which this research can be continued. The first of these directions is the expansion of the base of configurations that can be assessed with this procedure. There are many interesting variations of the standard case which have not yet been addressed. Included in this list are studies of the effect of:

- the tilting of the barrier both towards and away from the source.

- the possibility of raising the barrier above the ground such that there is a gap between the barrier and the ground.

- the angle at which the top section intersects the vertical. section on the T-shaped barrier (i.e. introducing barriers with "Y" and "arrow" shapes).

- the vertical positioning of the source, the number of sources and the relative strengths of these sources.

- using an average of a two dimensional field of receiver positions, rather than a single line. However, given the introductory nature of this work, it may be difficult to determine a relevant field of interest.

- the horizontal position of the source between parallel barrier in order to suggest different, but perhaps more feasible, designs for opposite sides of the road.

- the introduction of steps that will increase the complexity of the model such as a three-dimensional analyses, finite length barriers, the consideration of varying ground covers, atmospheric effects and the placement of other stationary objects such as buildings or embankments.

Each of these options offers a common opportunity to investigate the design of the barrier and its placement for improved attenuative performance above and beyond that obtained in the cases investigated here.

Another course of action involves recognizing that the results obtained in this paper suggest that there is great potential for the development of this procedure. The development of this procedure could result in the evolution of a valuable wave-based reference model for rating a barrier's performance. A set of quick reference tables that would provide correction factors for the geometrical parameters of the design configuration is quite possible. This system could then

be a universal technique that permits a easy and accurate comparison of relatively dissimilar designs.

APPENDIX A - FIGURES

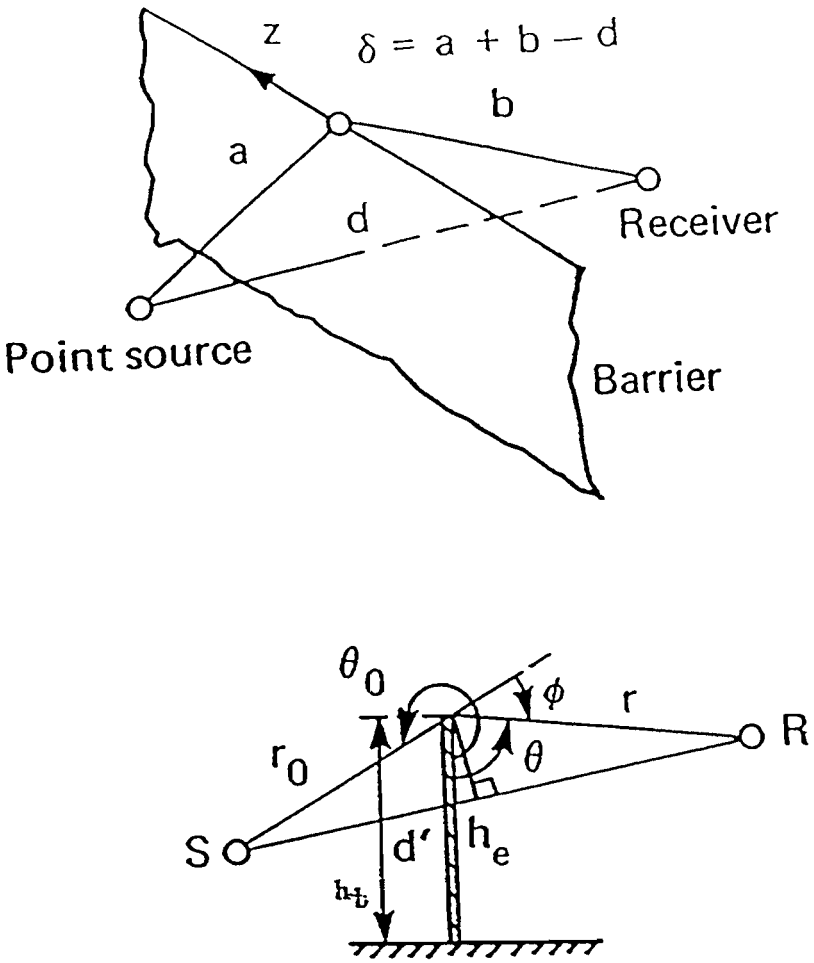

Figure 1 - Definition of Geometrical Parameters

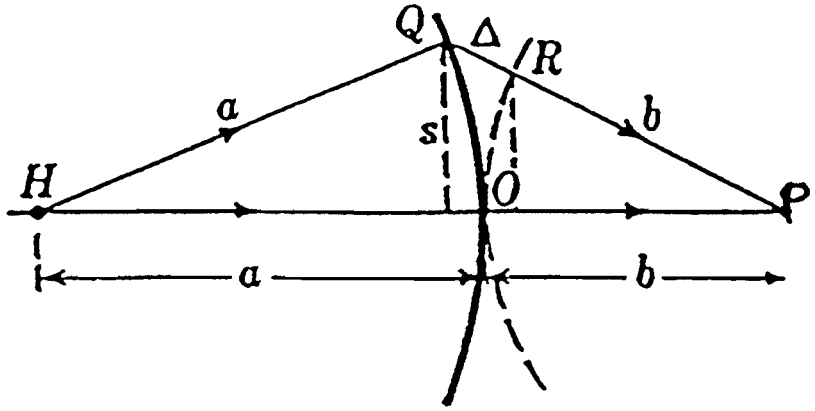

Figure 2 - Path Length Difference

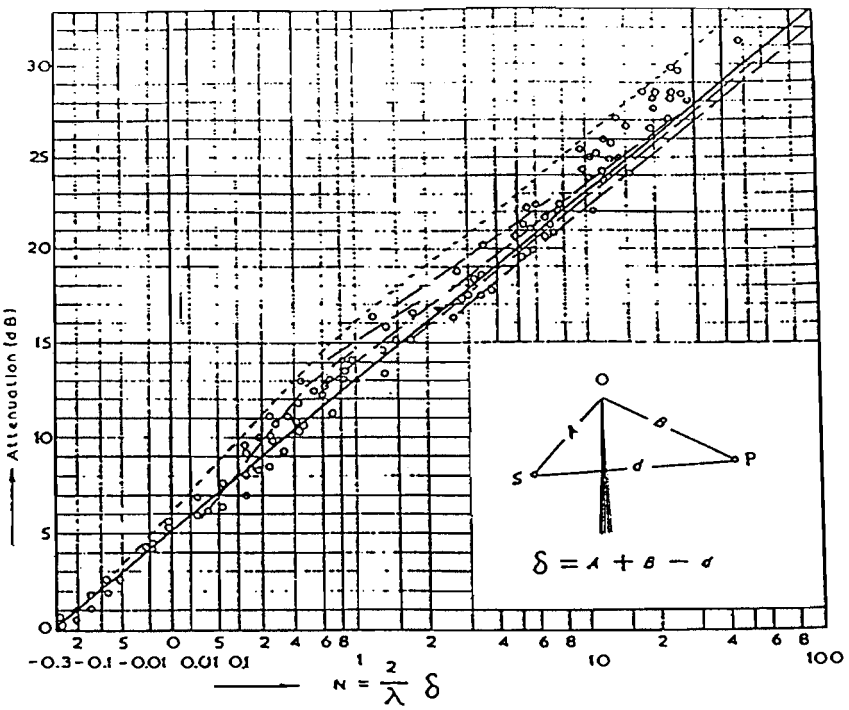

Figure 3 - Maekawa's Chart

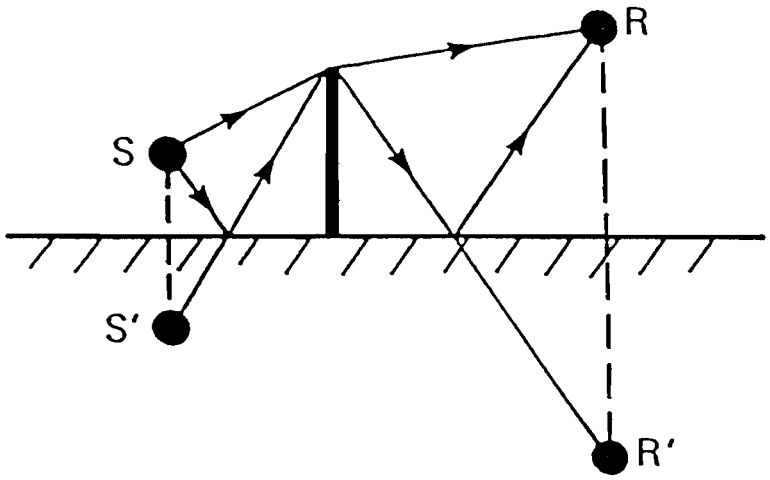

Figure 4 - Multiple Propagation Paths

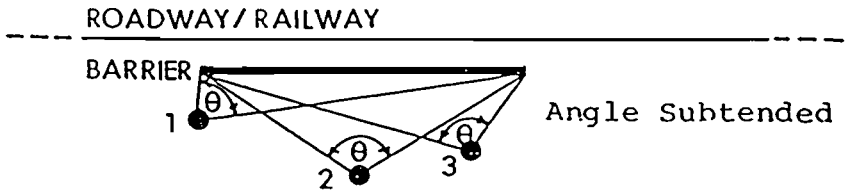

Figure 5 - Subtended Angle - Hand Method

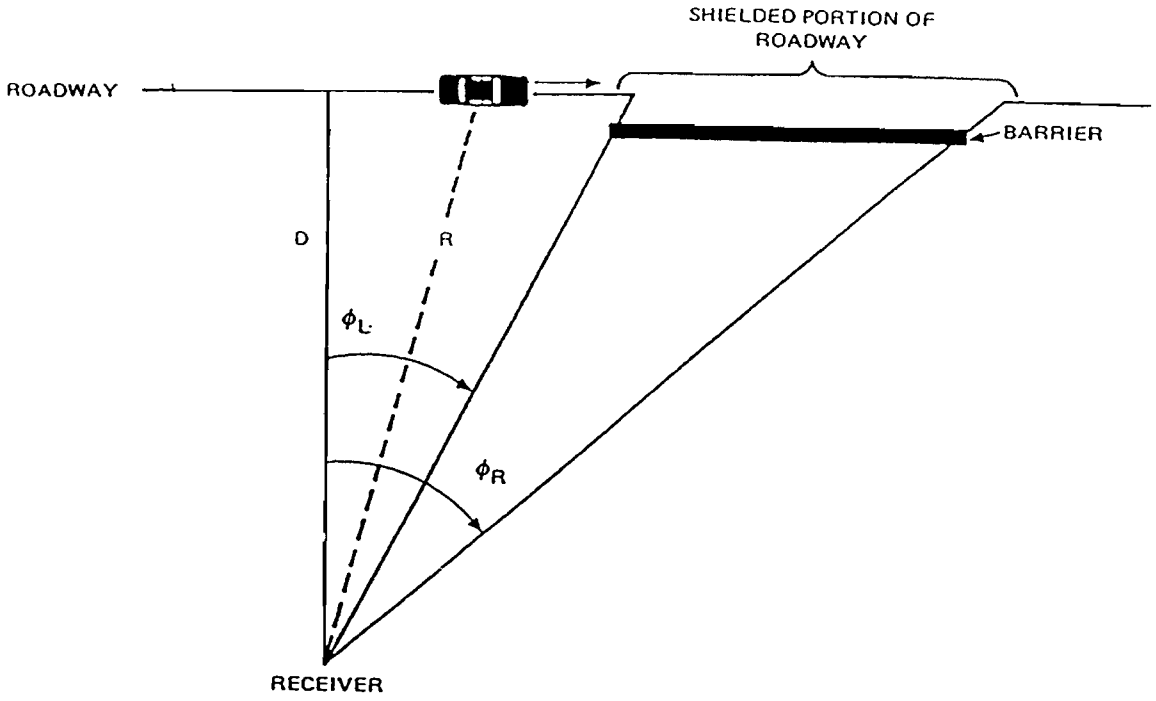

Figure 6 - Subtended Angles - FHWA method

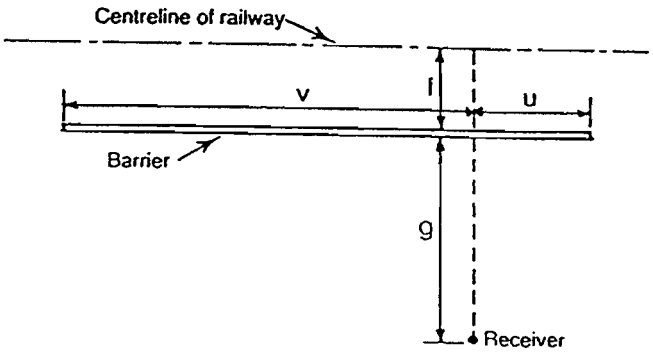

Figure 7 - CHMC Barrier Length Ratio

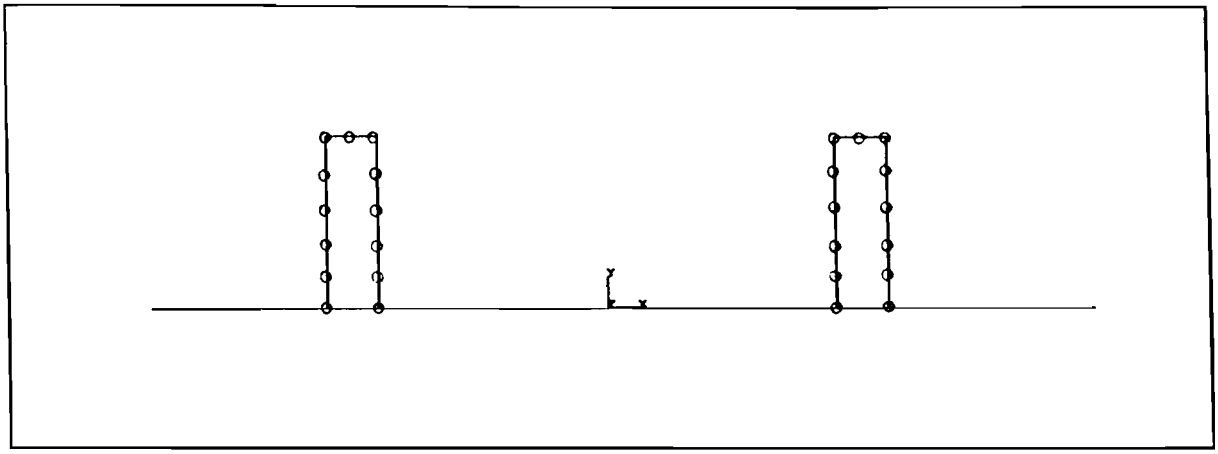

Figure 8 - Sample BEM Preprocessing Mesh

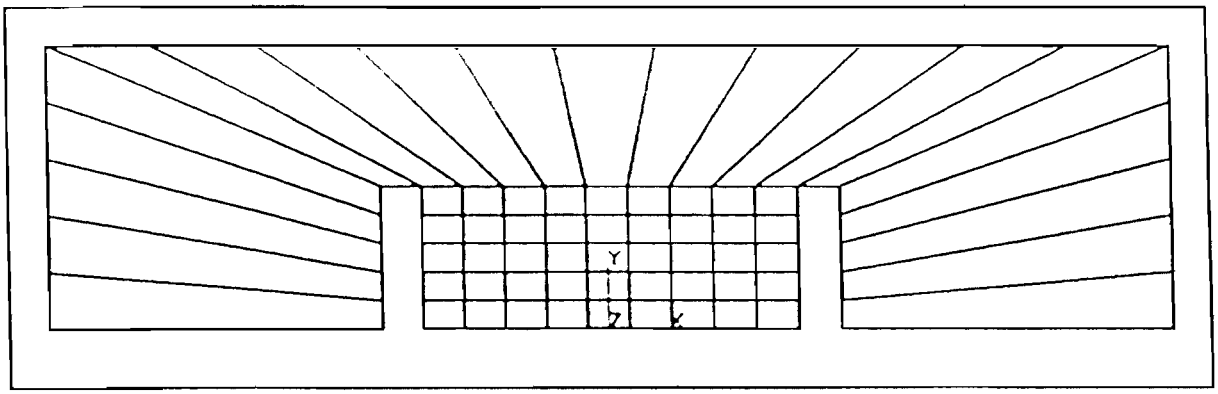

Figure 9 - Sample FEM Preprocessing Mesh

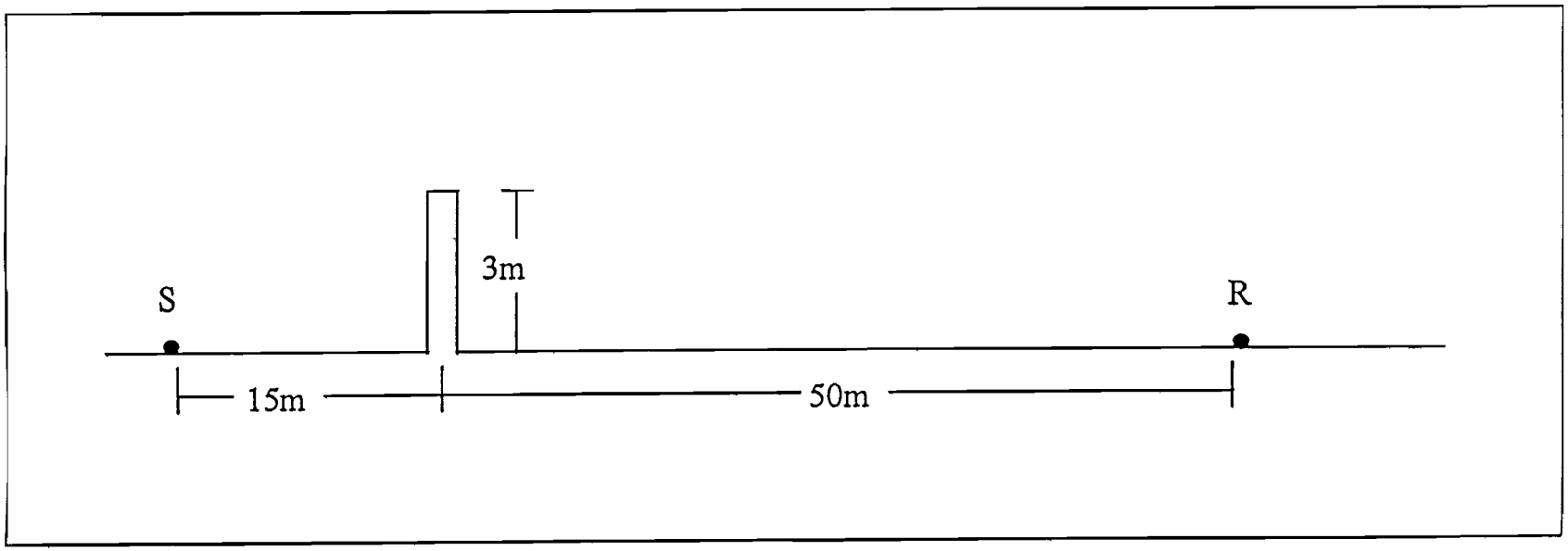

Figure 10 - Hothersall Geometry - Receiver on Ground

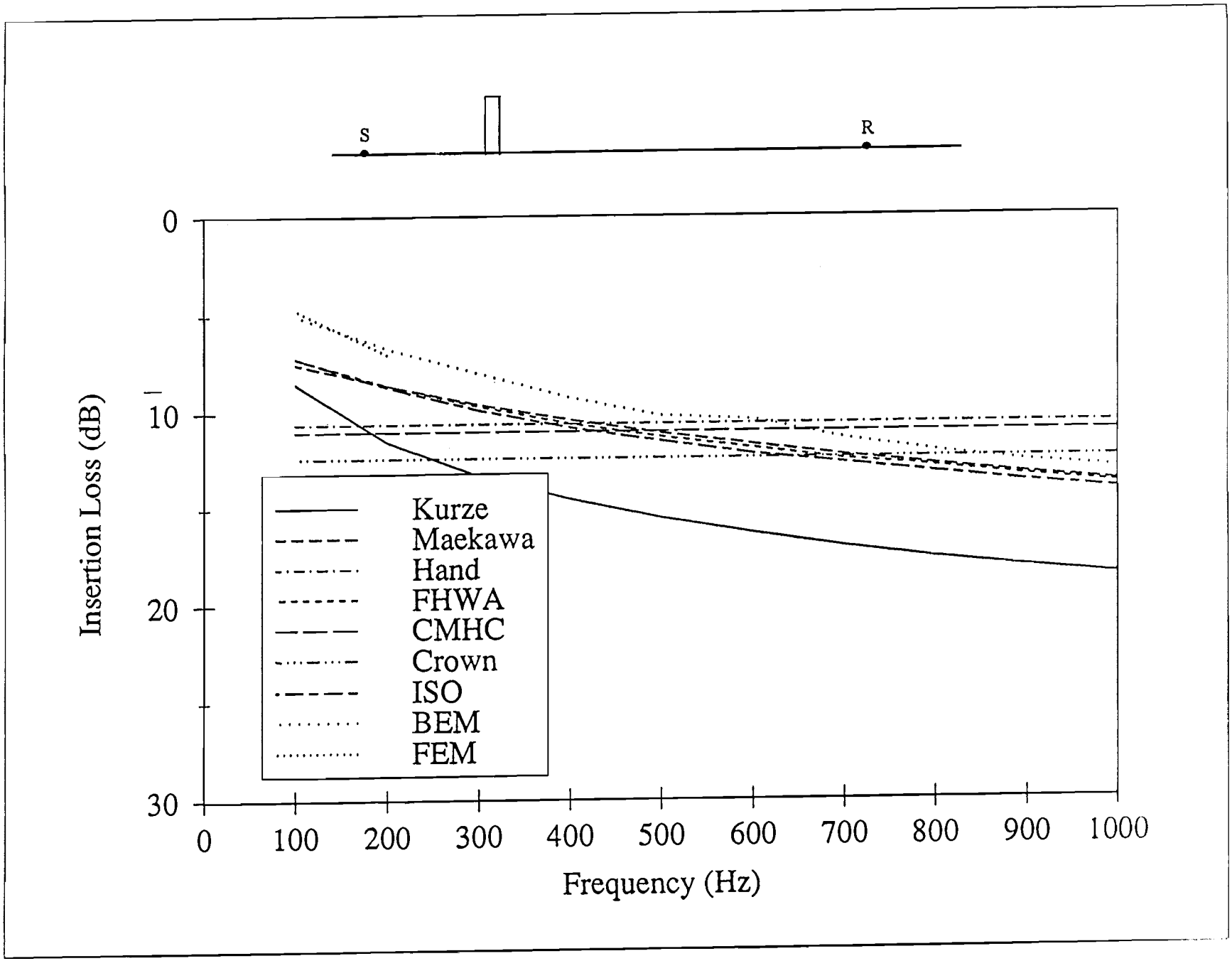

Figure 11 - Frequency Sweep of Hothersall Geometry

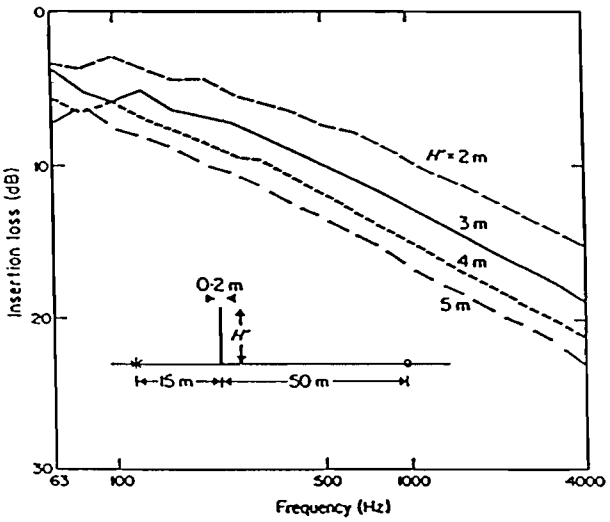

Figure 12 - Hothersall Evaluation

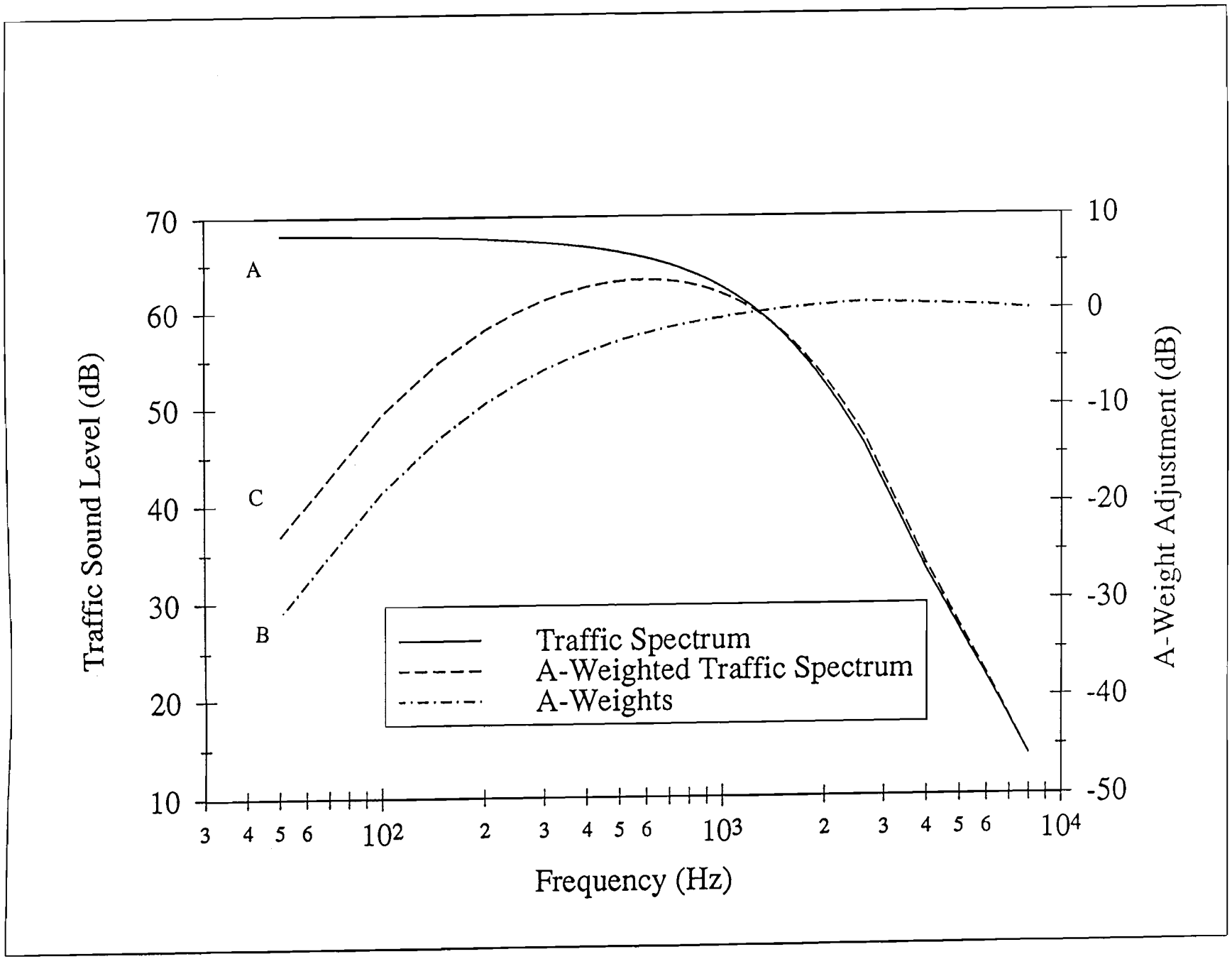

Figure 13 - A-Weighted Traffic Spectrum

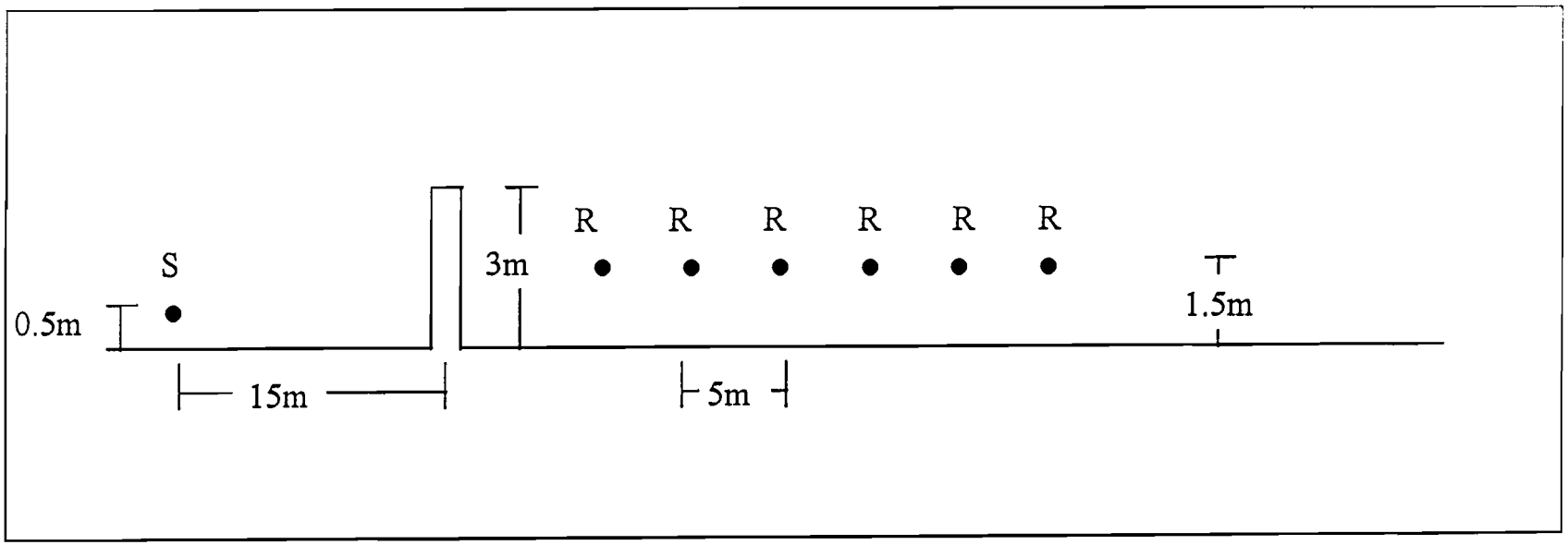

Figure 14 - The Standard Geometry

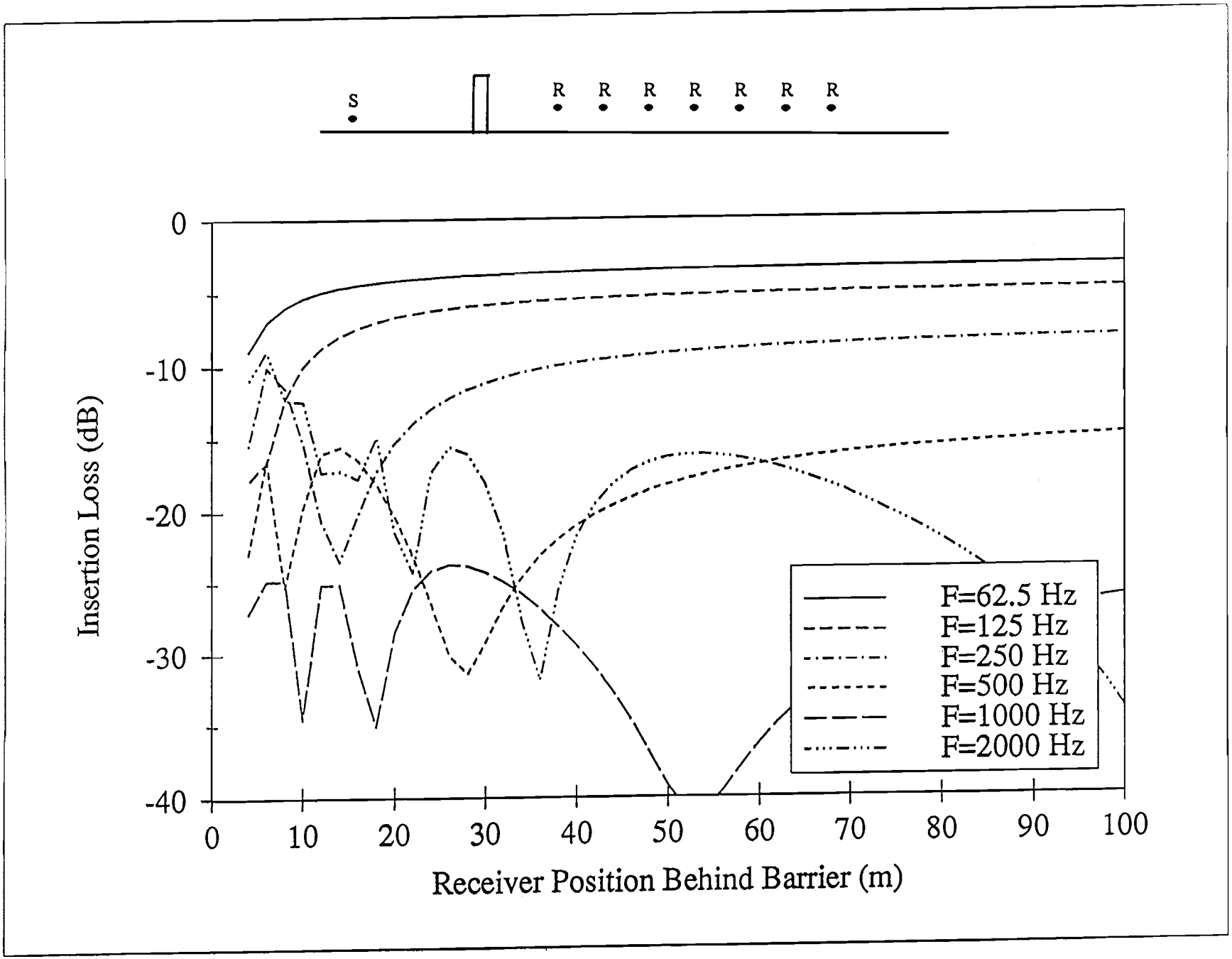

Figure 15 - Insertion Loss vs. Distance for Standard Geometry

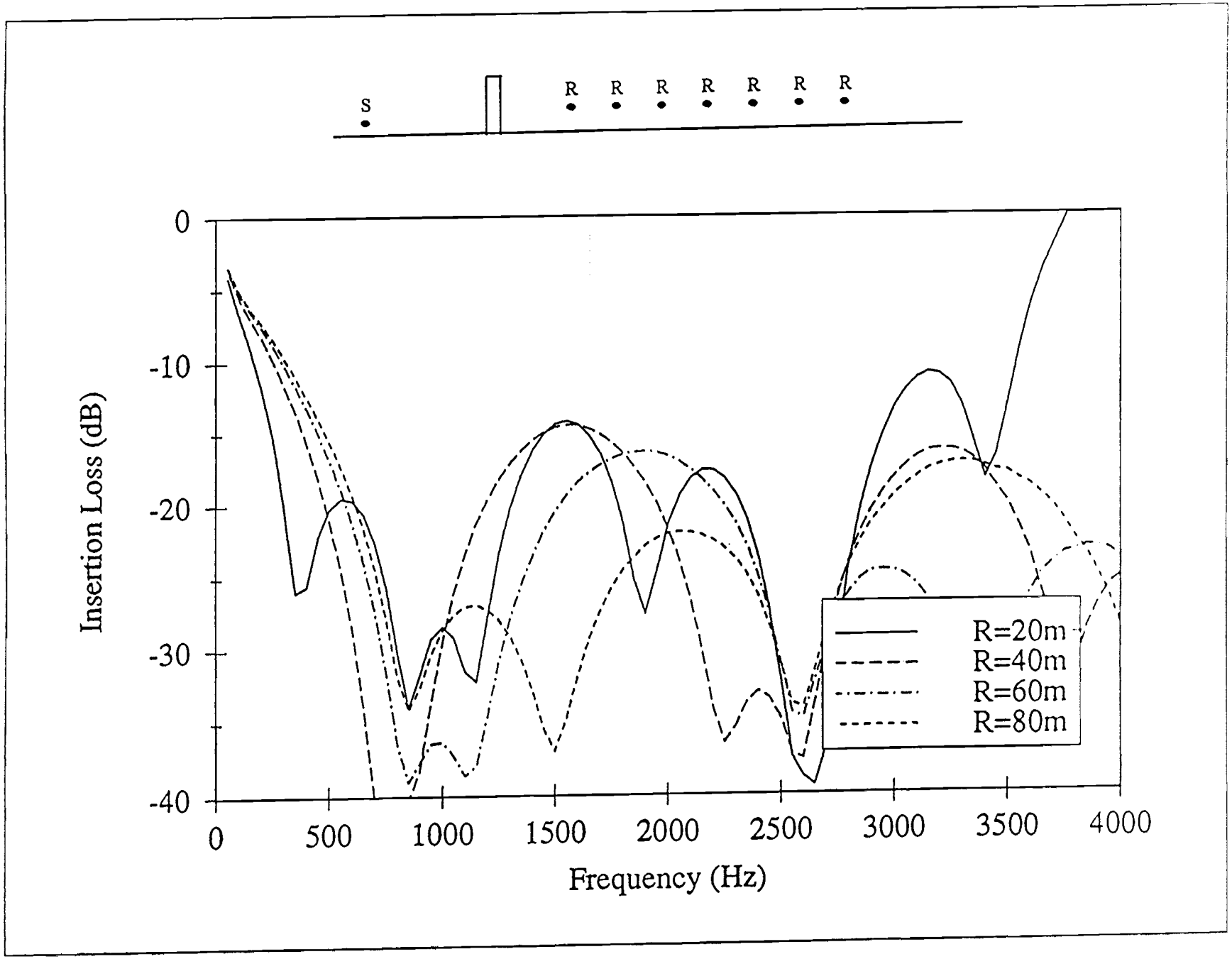

Figure 16 - Insertion Loss vs. Frequency for Standard Geometry

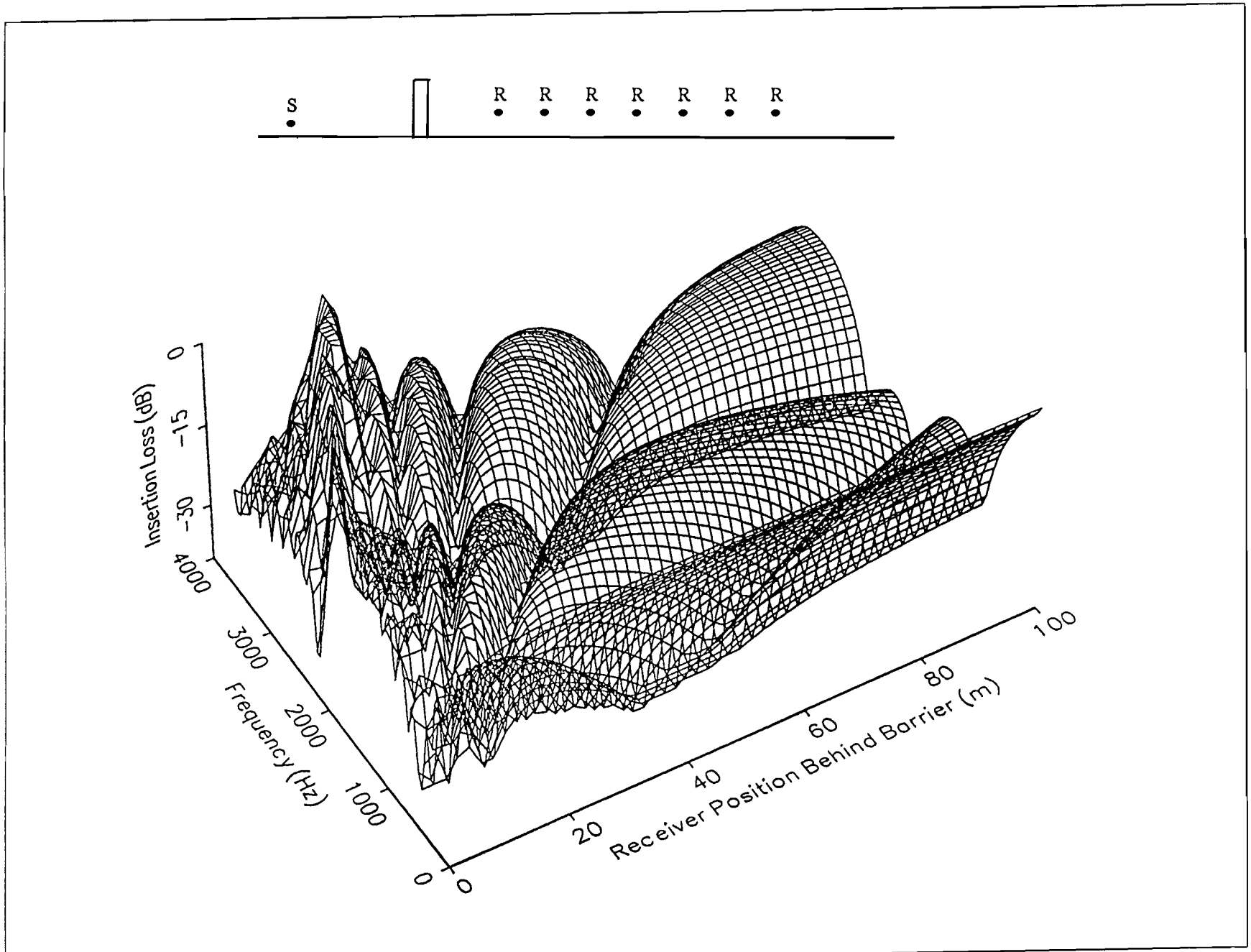

Figure 17 - Insertion Loss vs. Distance and Frequency

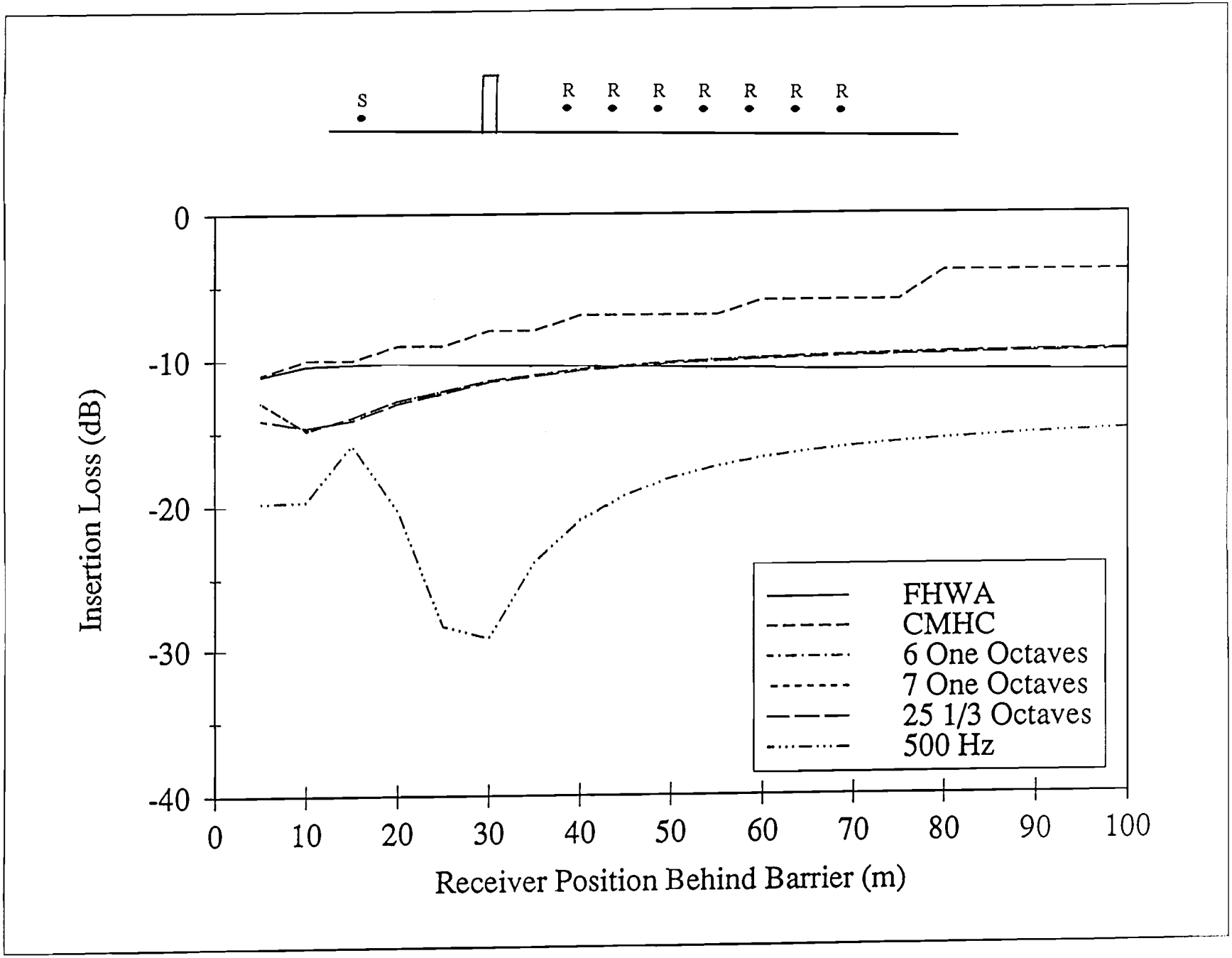

Figure 18 - Ray Based vs. Frequency Weighted Insertion Loss Curve

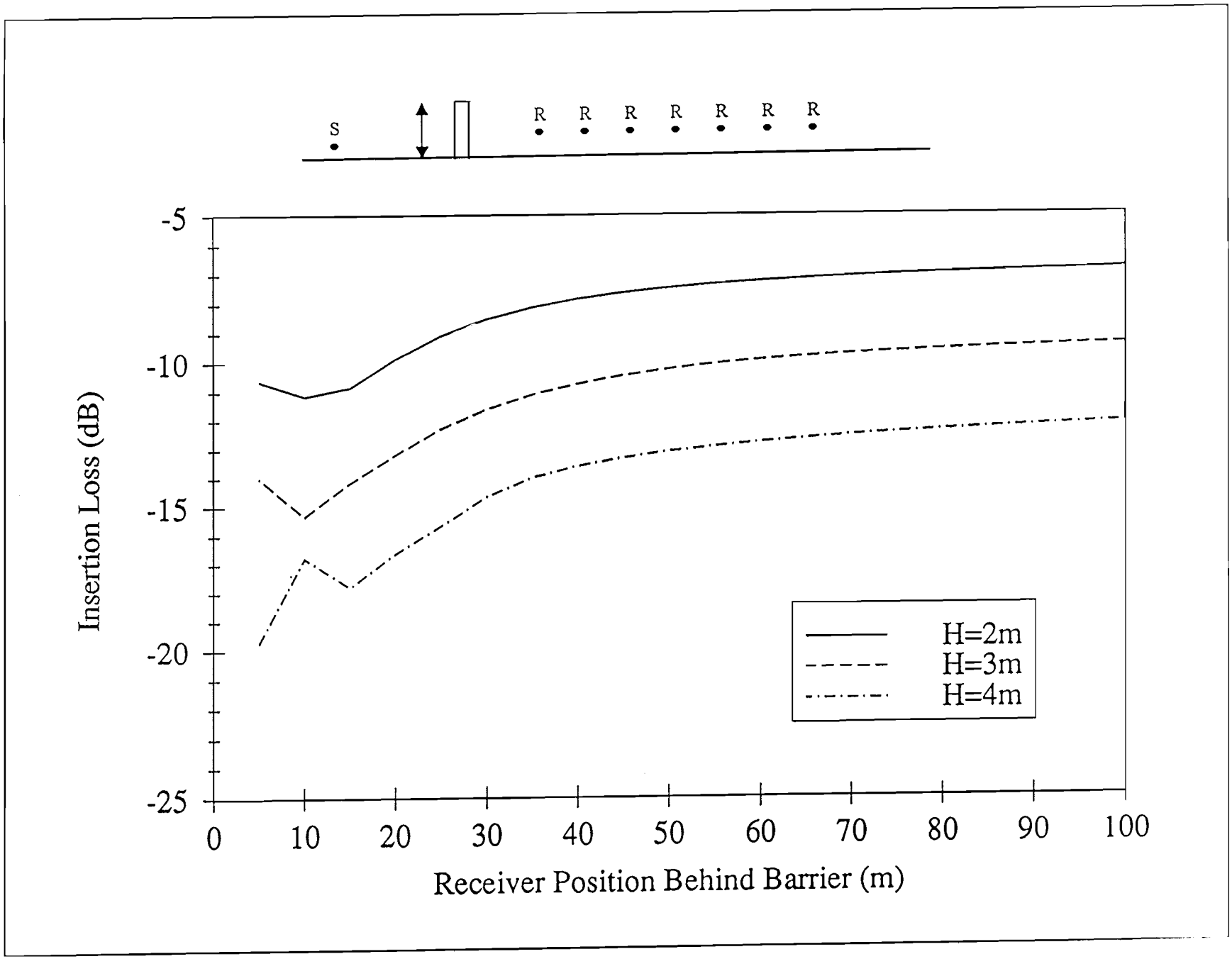

Figure 19 - Effect of Varying Height

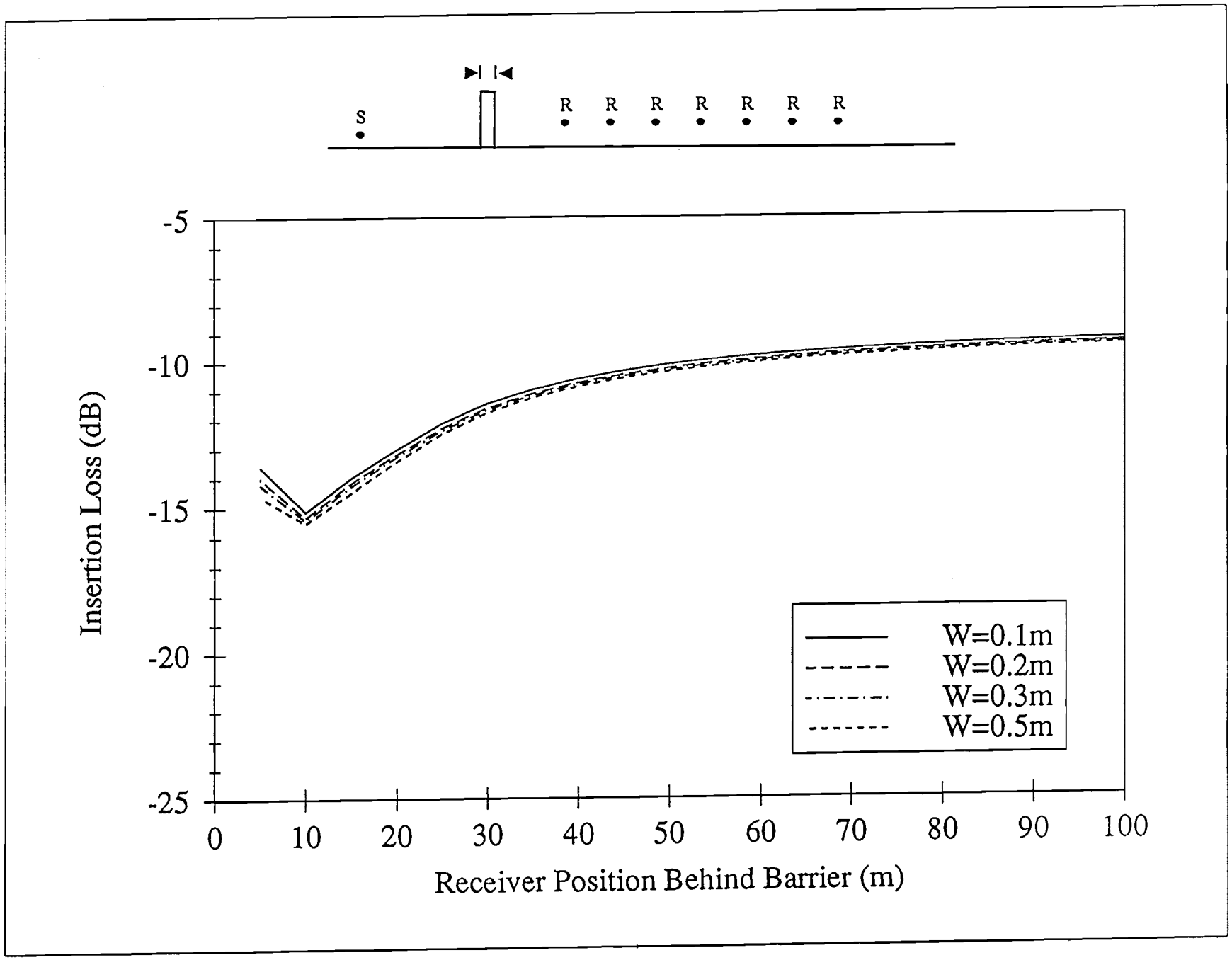

Figure 20 - Effect of Varying Width

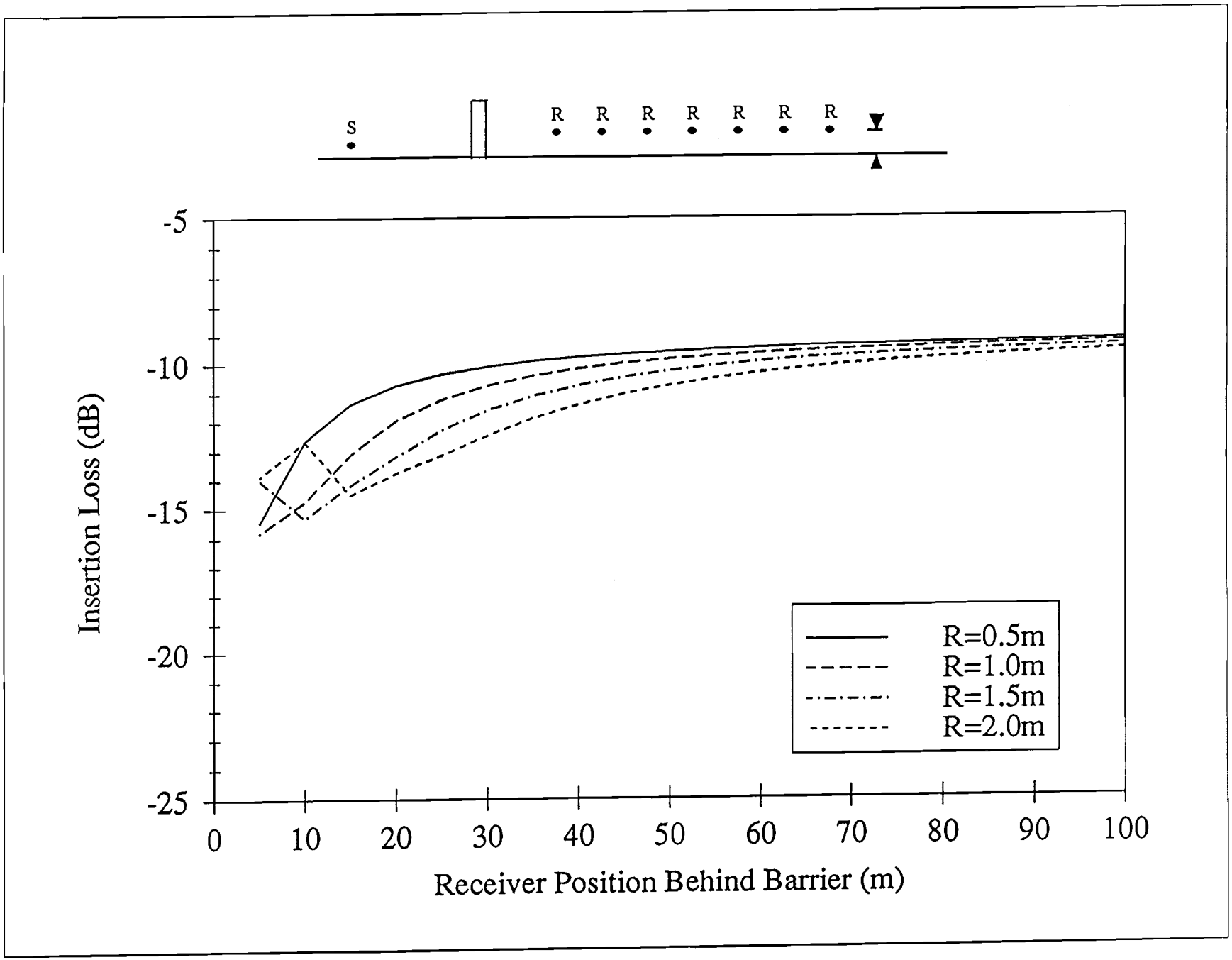

Figure 21 - Effect of Varying Receiver Height

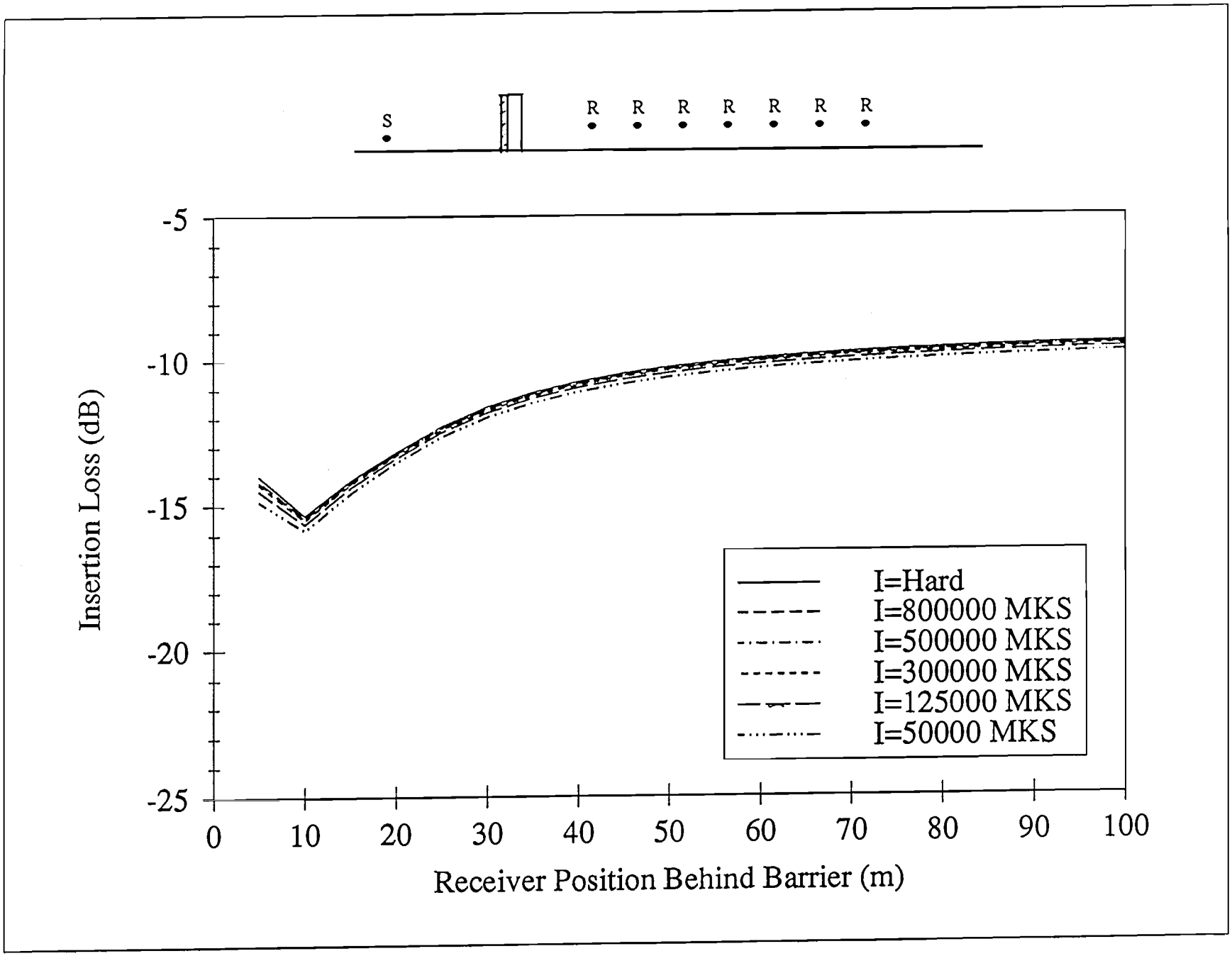

Figure 22 - Effect of Adding Absorptive Coating

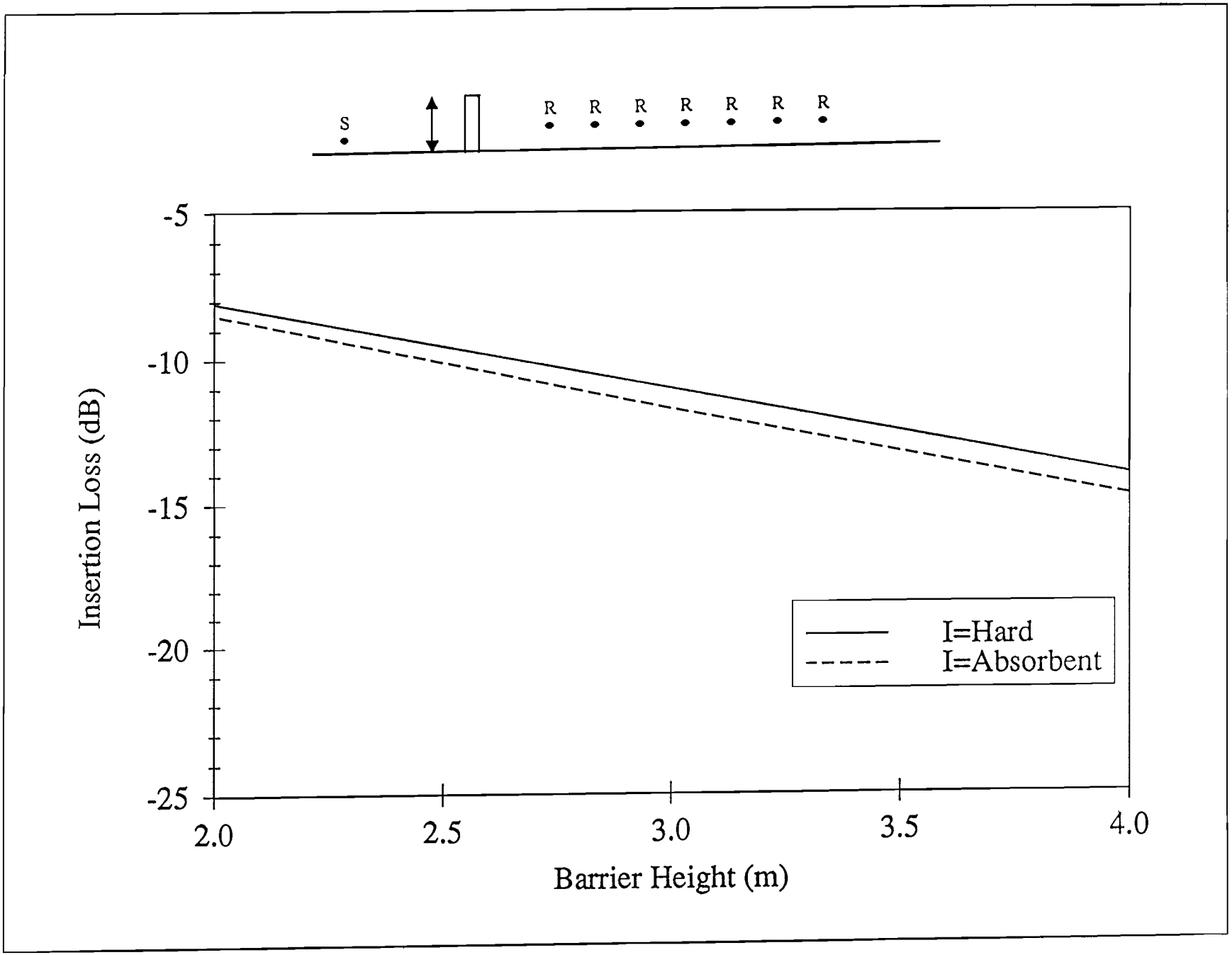

Figure 23 - Insertion Loss vs. Height

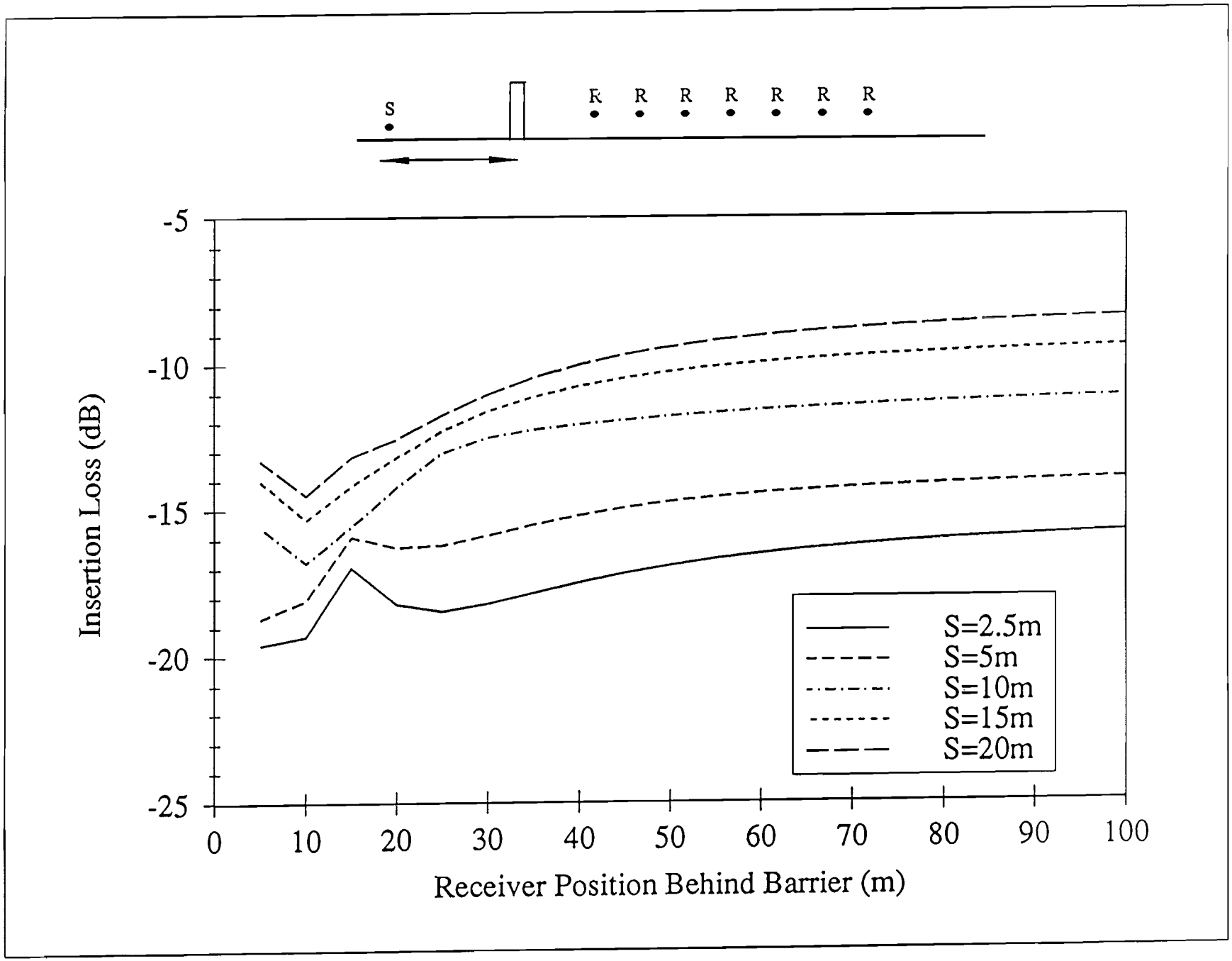

Figure 24 - Effect of Varying Source Position

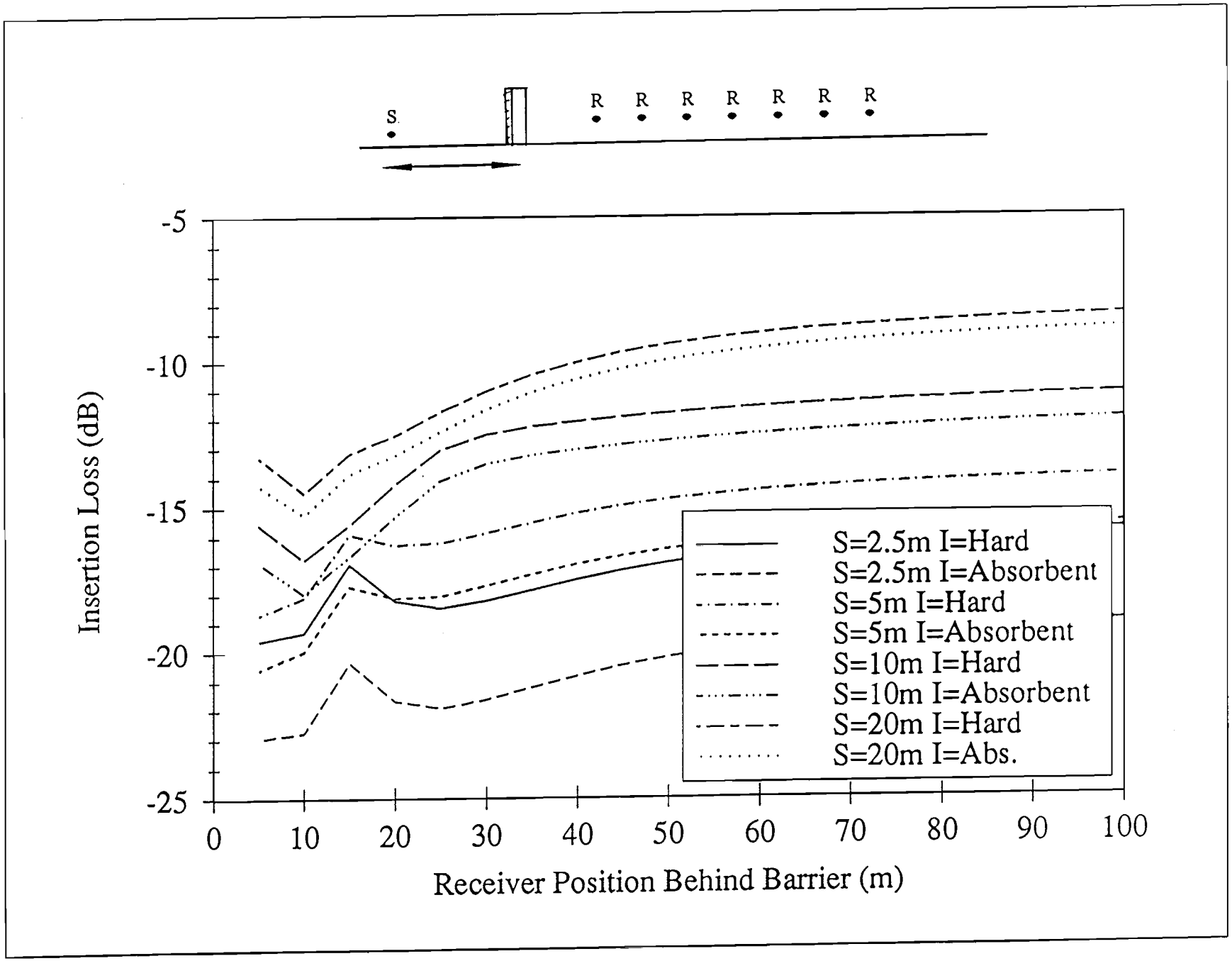

Figure 25 - Effect of Absorption with Varying Source Position

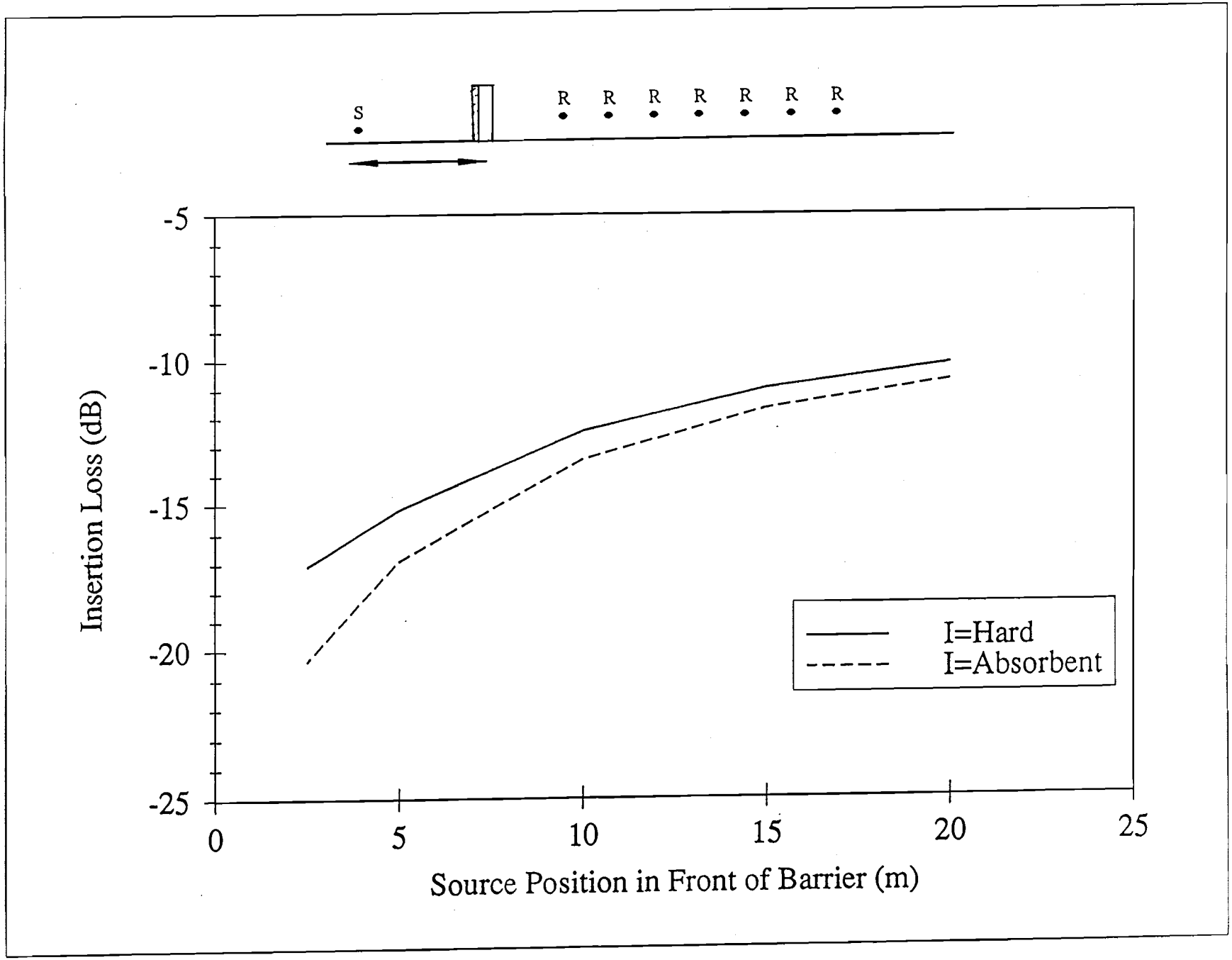

Figure 26 - Insertion Loss vs. Source Position

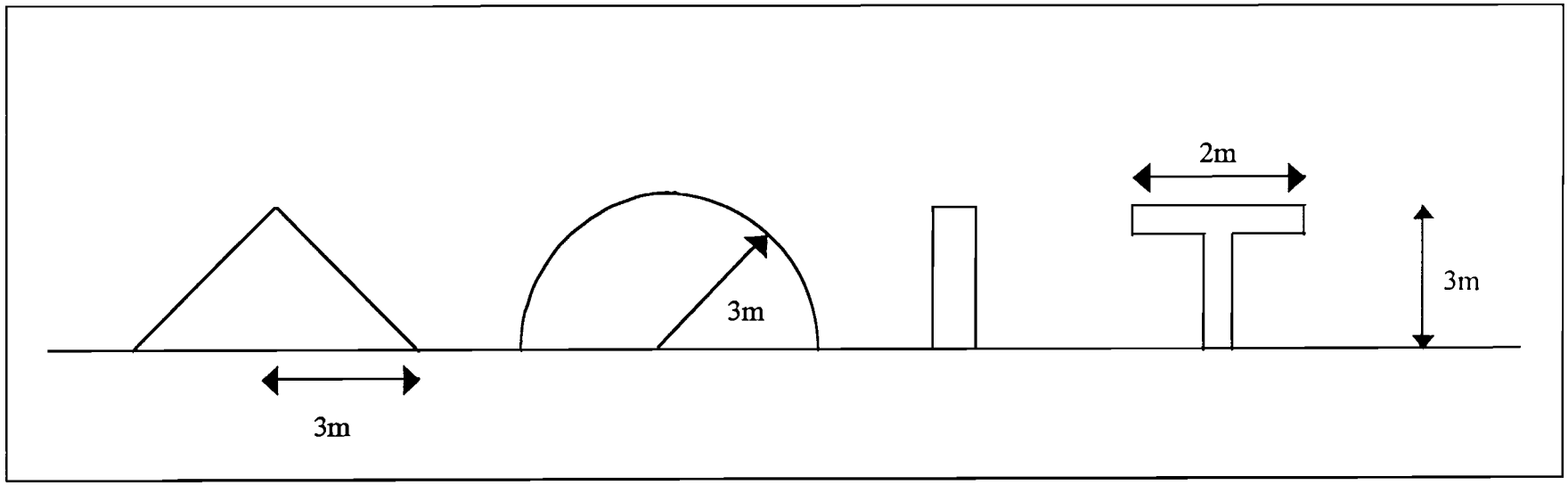

Figure 27 - Alternate Barrier Design

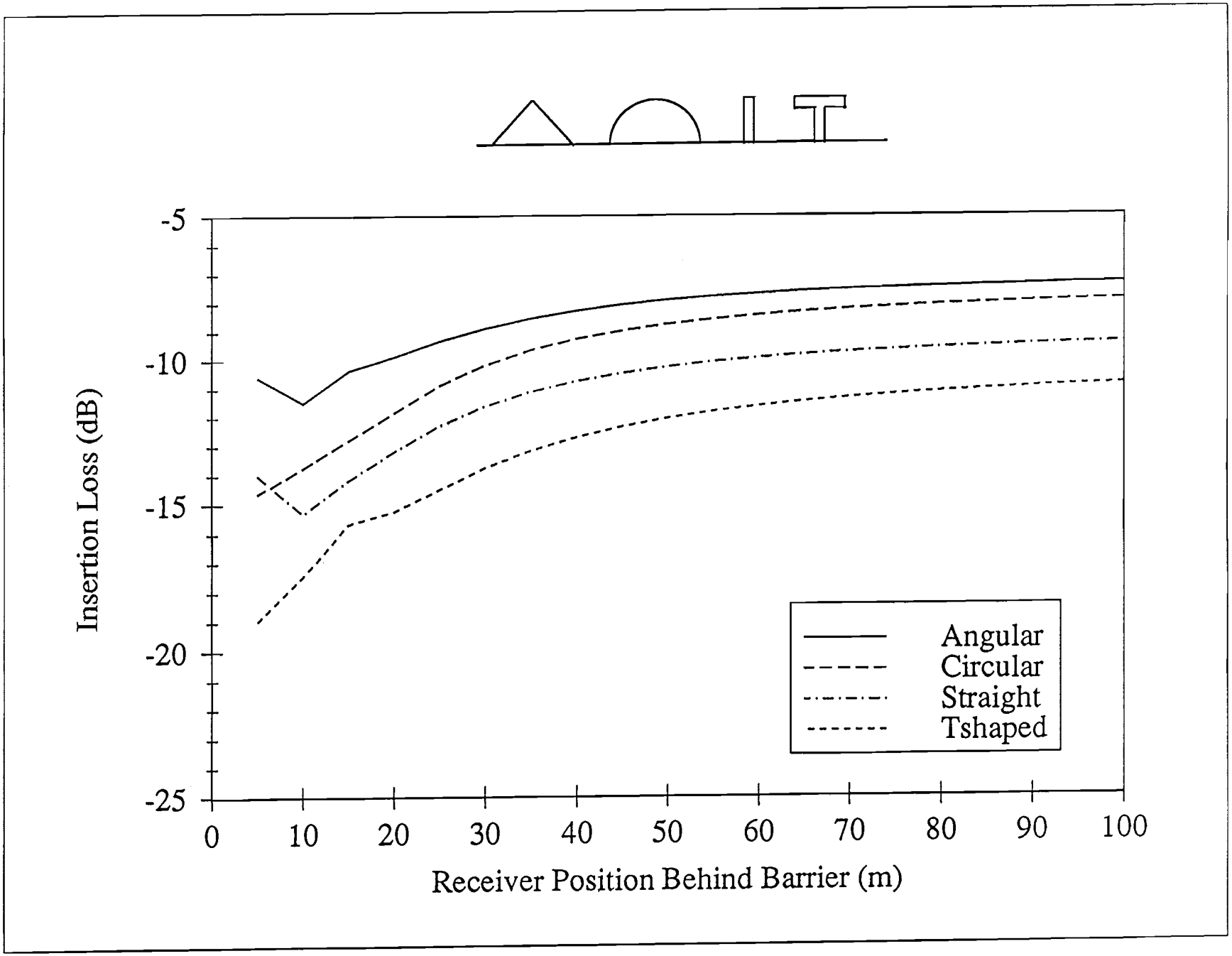

Figure 28 - Effect of Barrier Shape

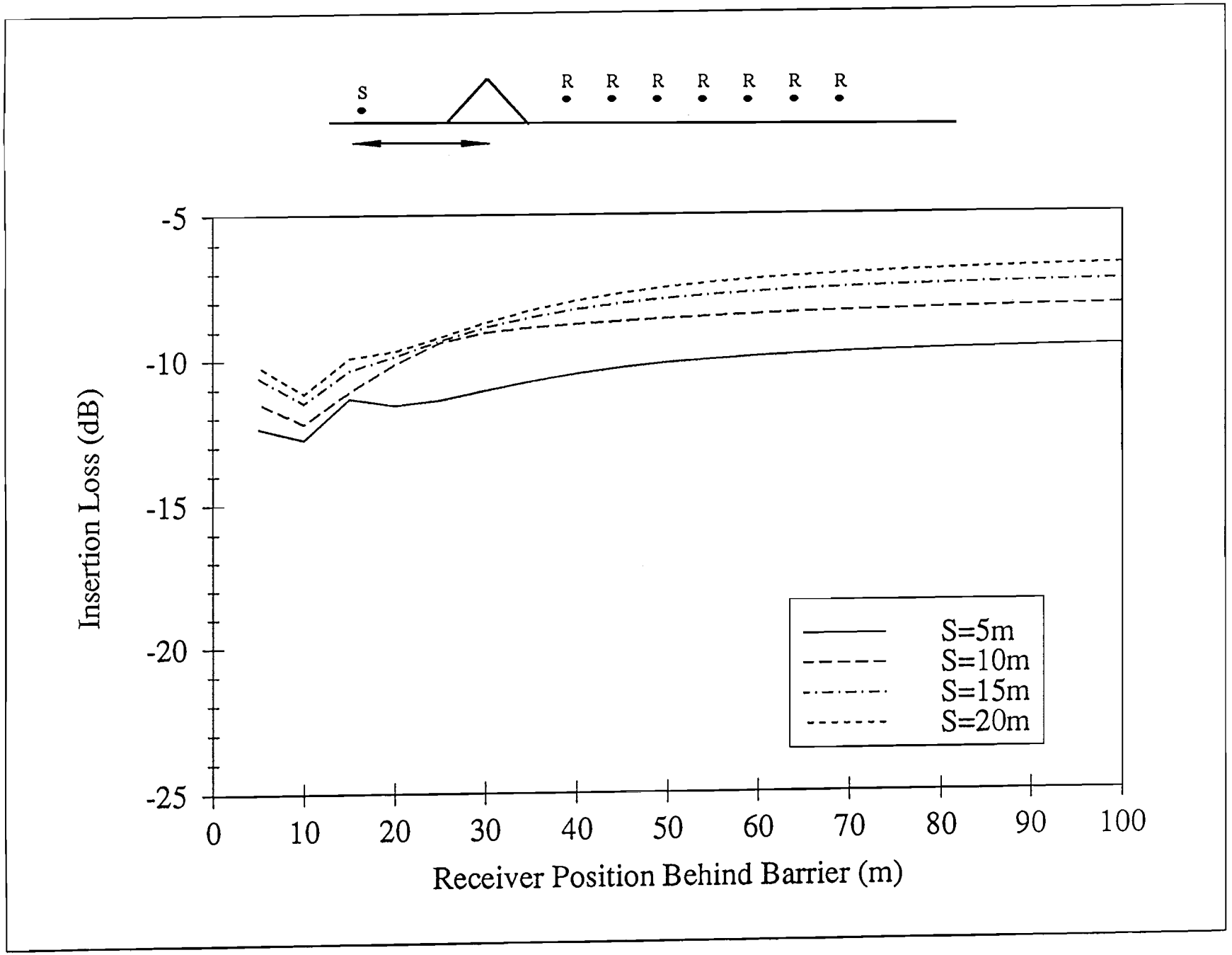

Figure 29 - Effect of Varying Source Position in Front of Angular Barrier

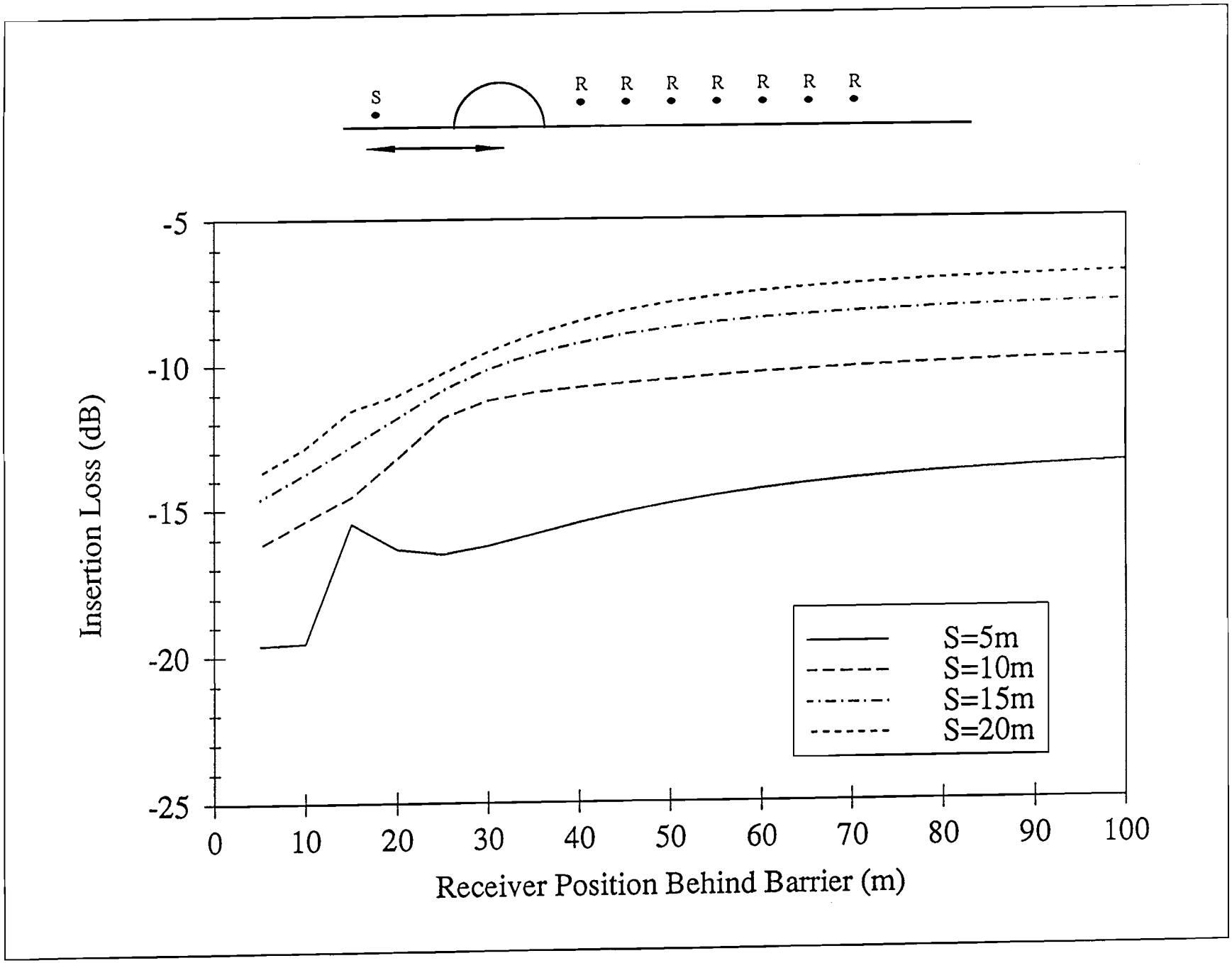

Figure 30 - Effect of Varying Source Position in Front of Circular Barrier

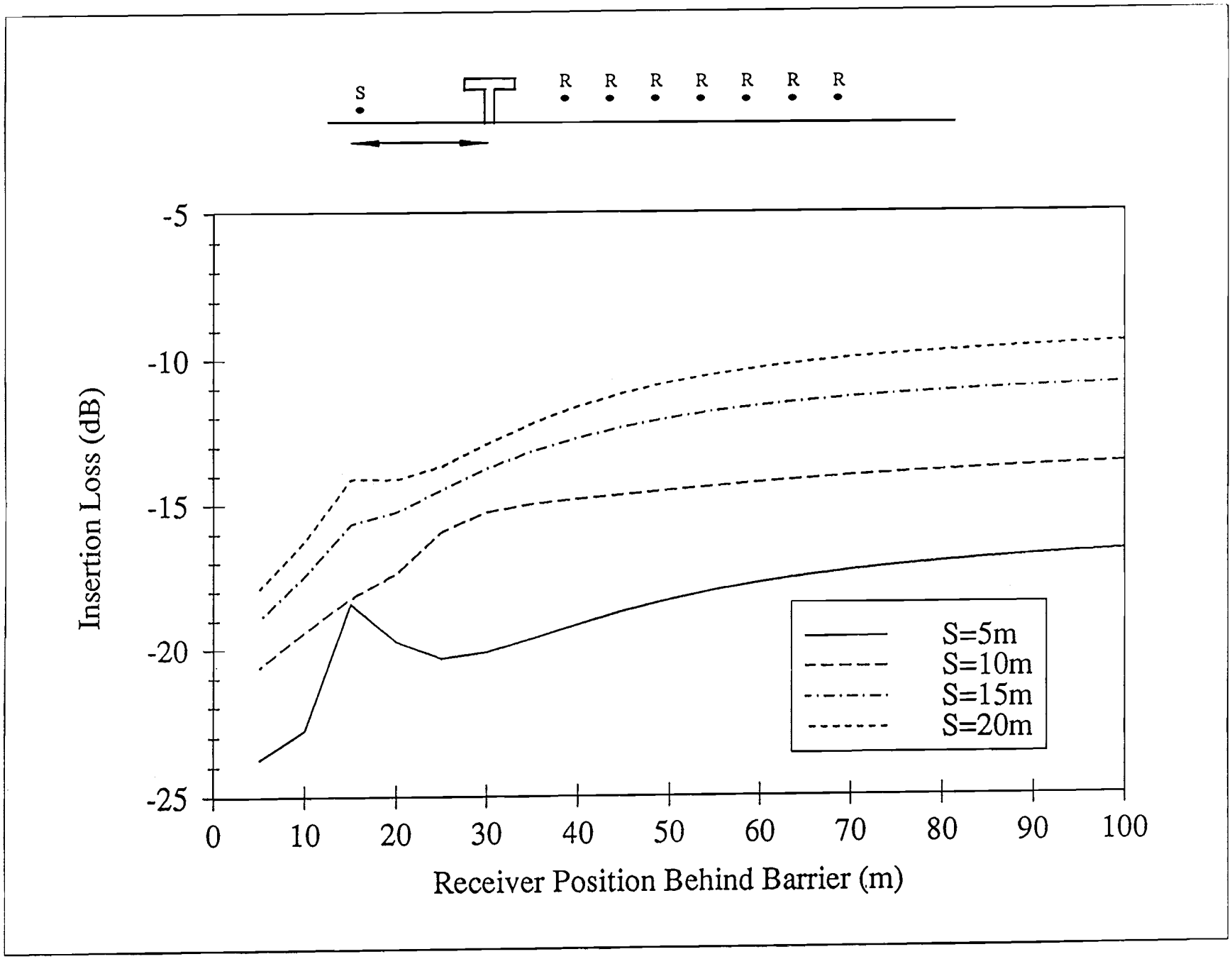

Figure 31 - Effect of Varying Source Position in Front of T-Shaped Barrier

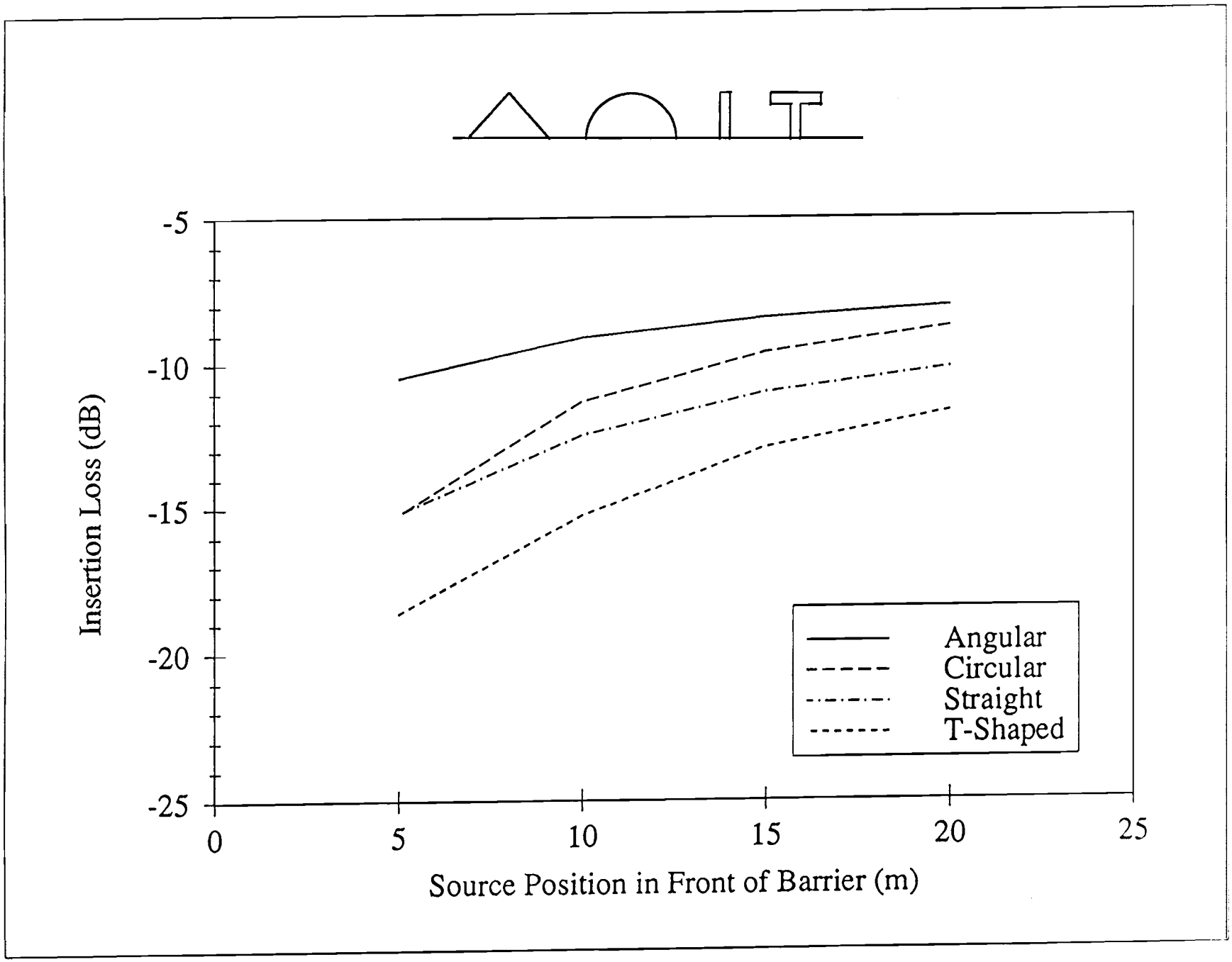

Figure 32 - Insertion Loss vs. Source Position for Varying Design

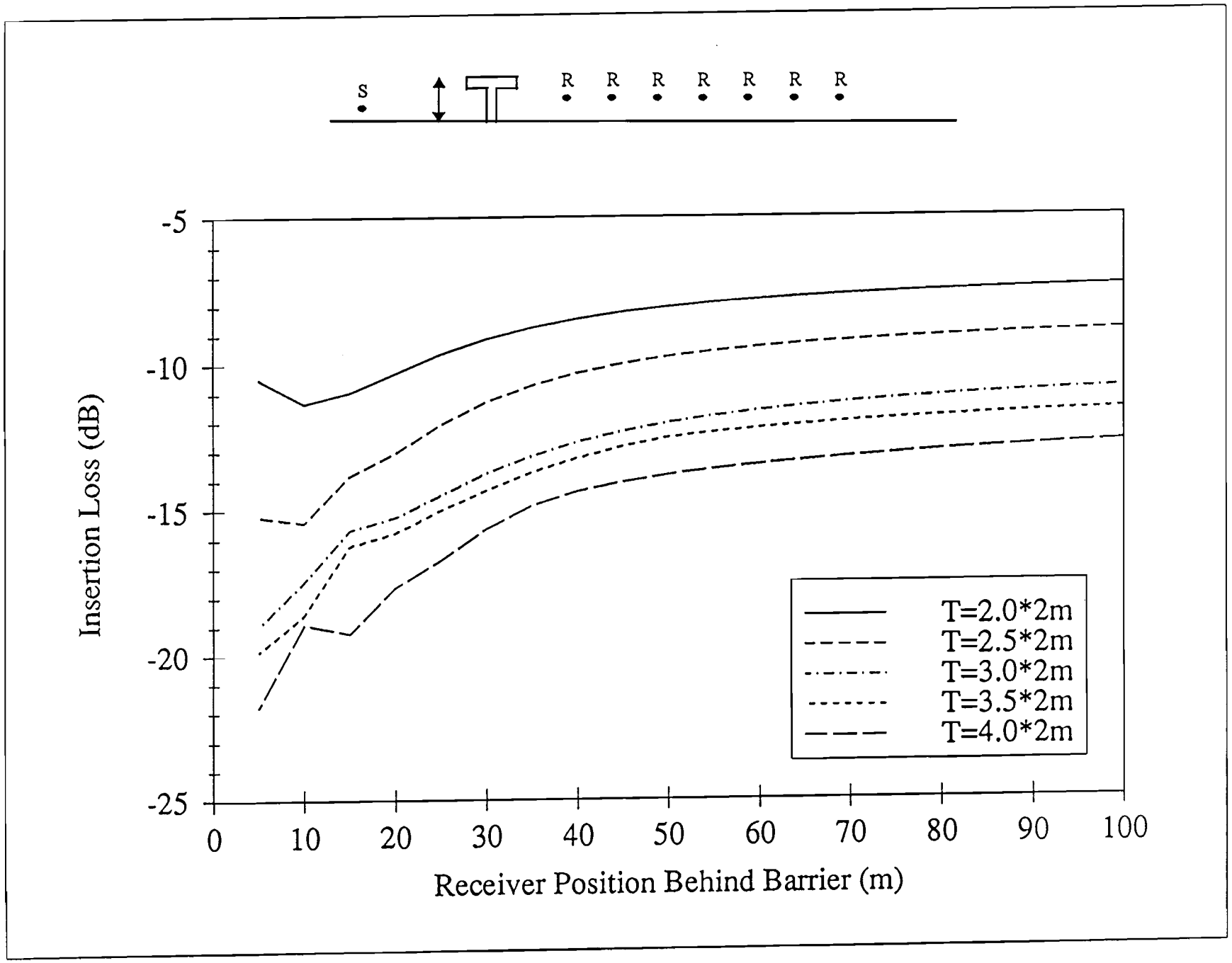

Figure 33 - Effect of Varying Height of T-Shaped Barrier

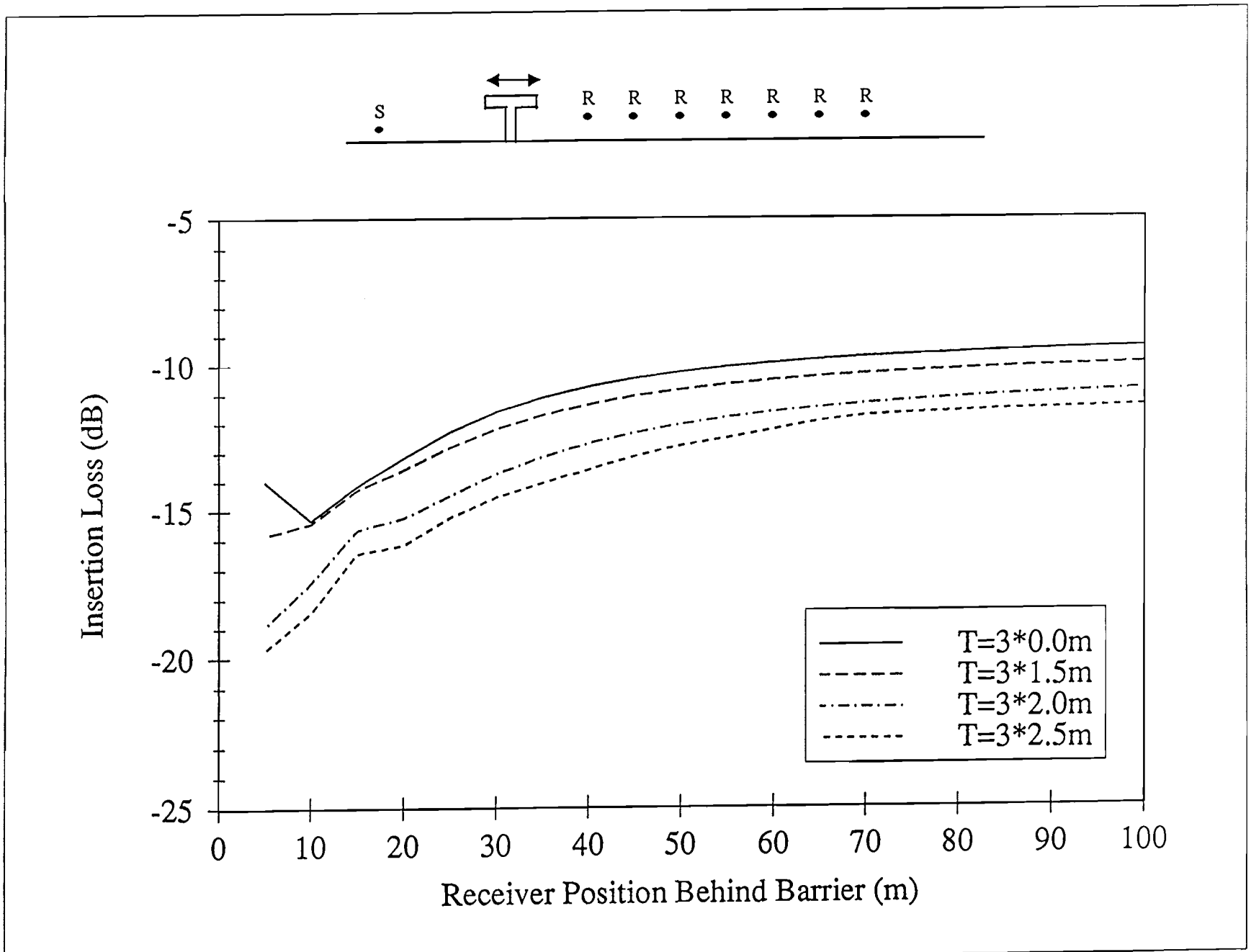

Figure 34 - Effect of Varying Length of Top of T-Shaped Barrier

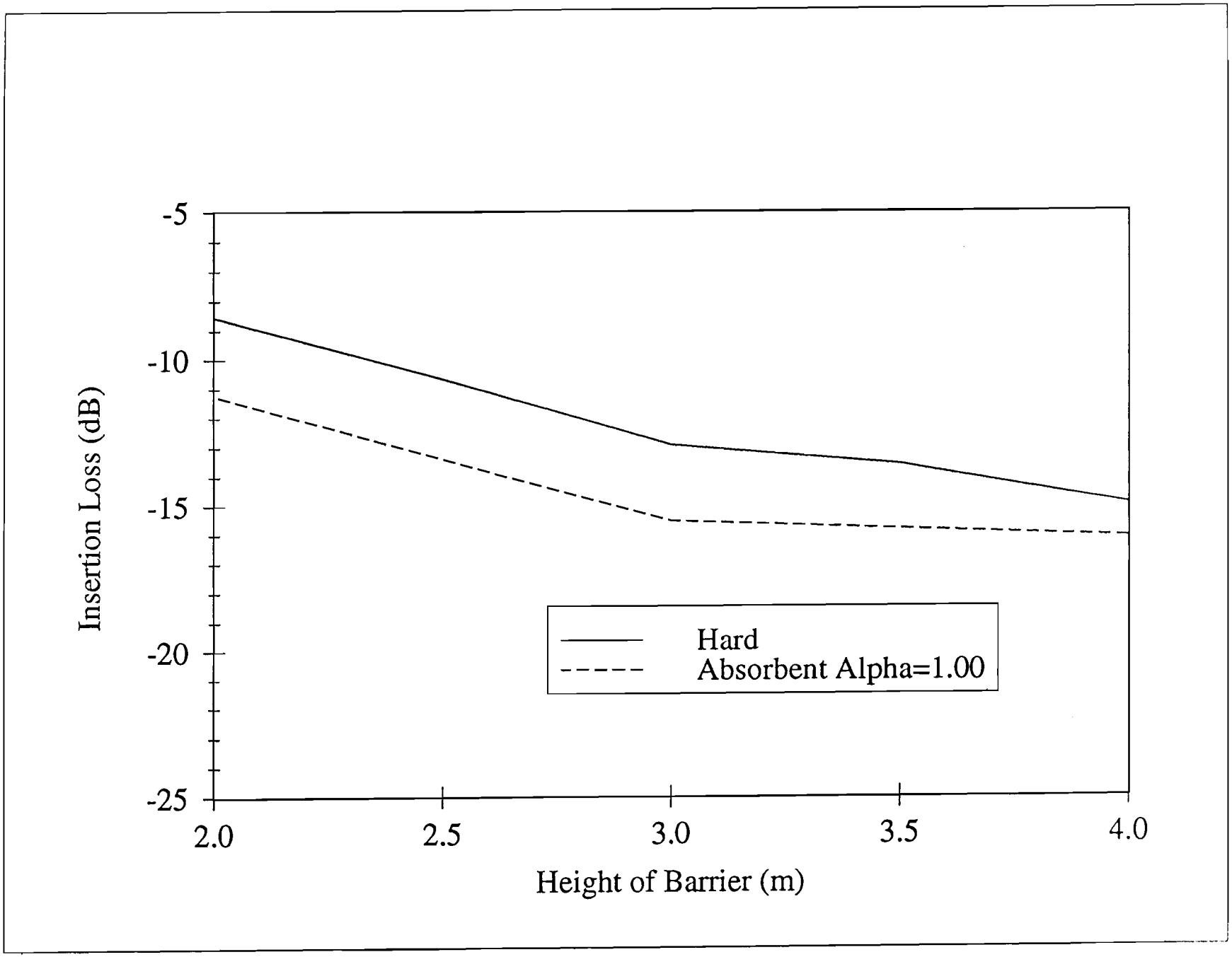

Figure 35 - Insertion Loss vs. Height of T-Shaped Barrier

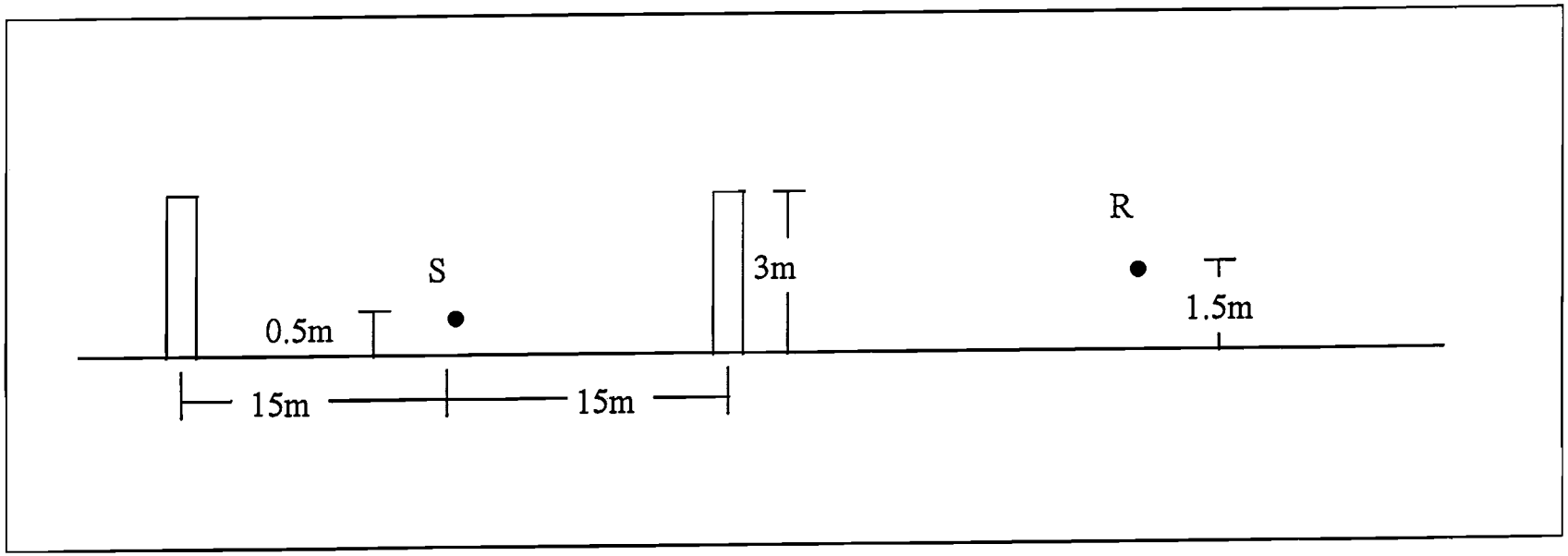

Figure 36 - Parallel Barrier Configuration

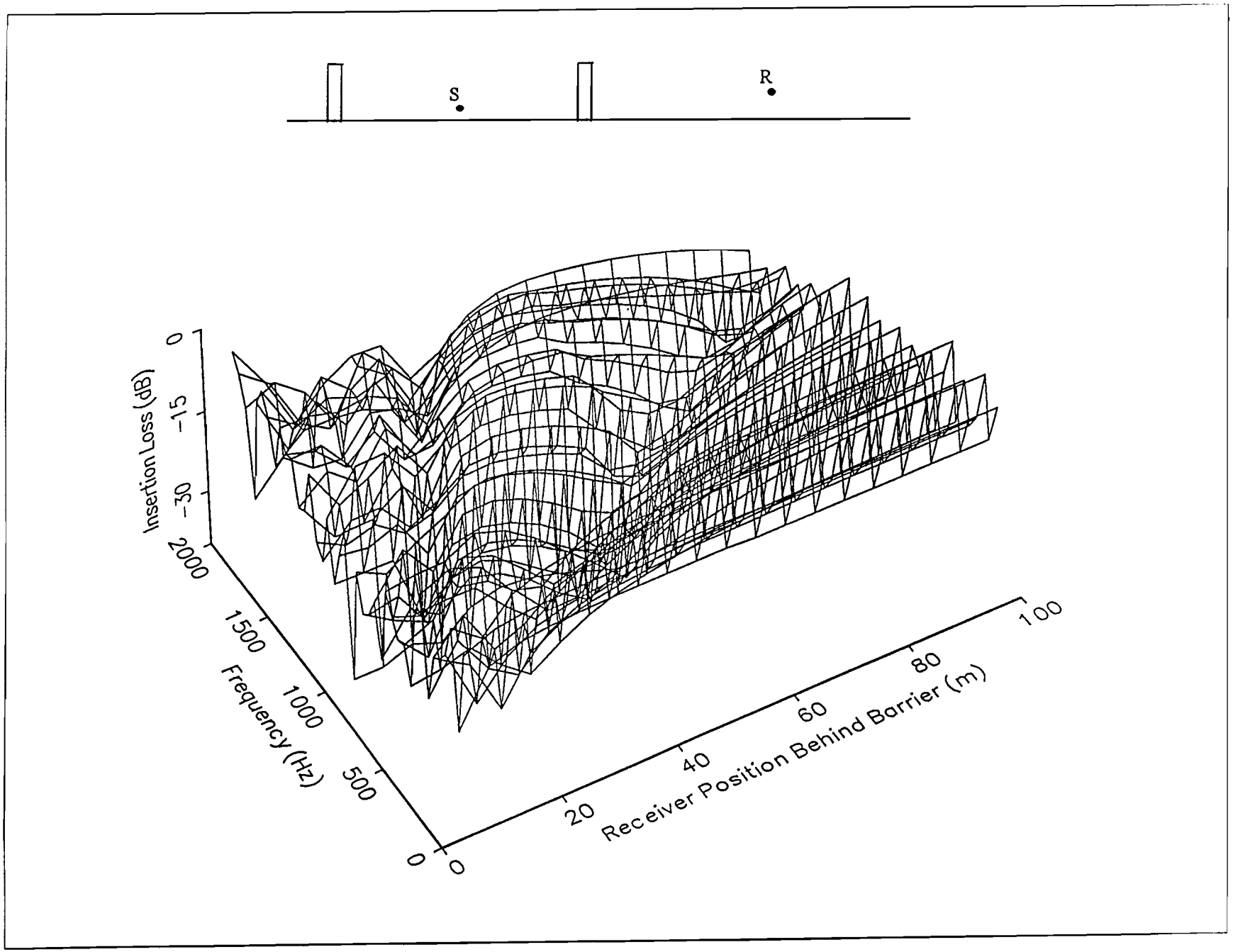

Figure 37 - Insertion Loss vs. Frequency vs. Distance for Parallel Barrier

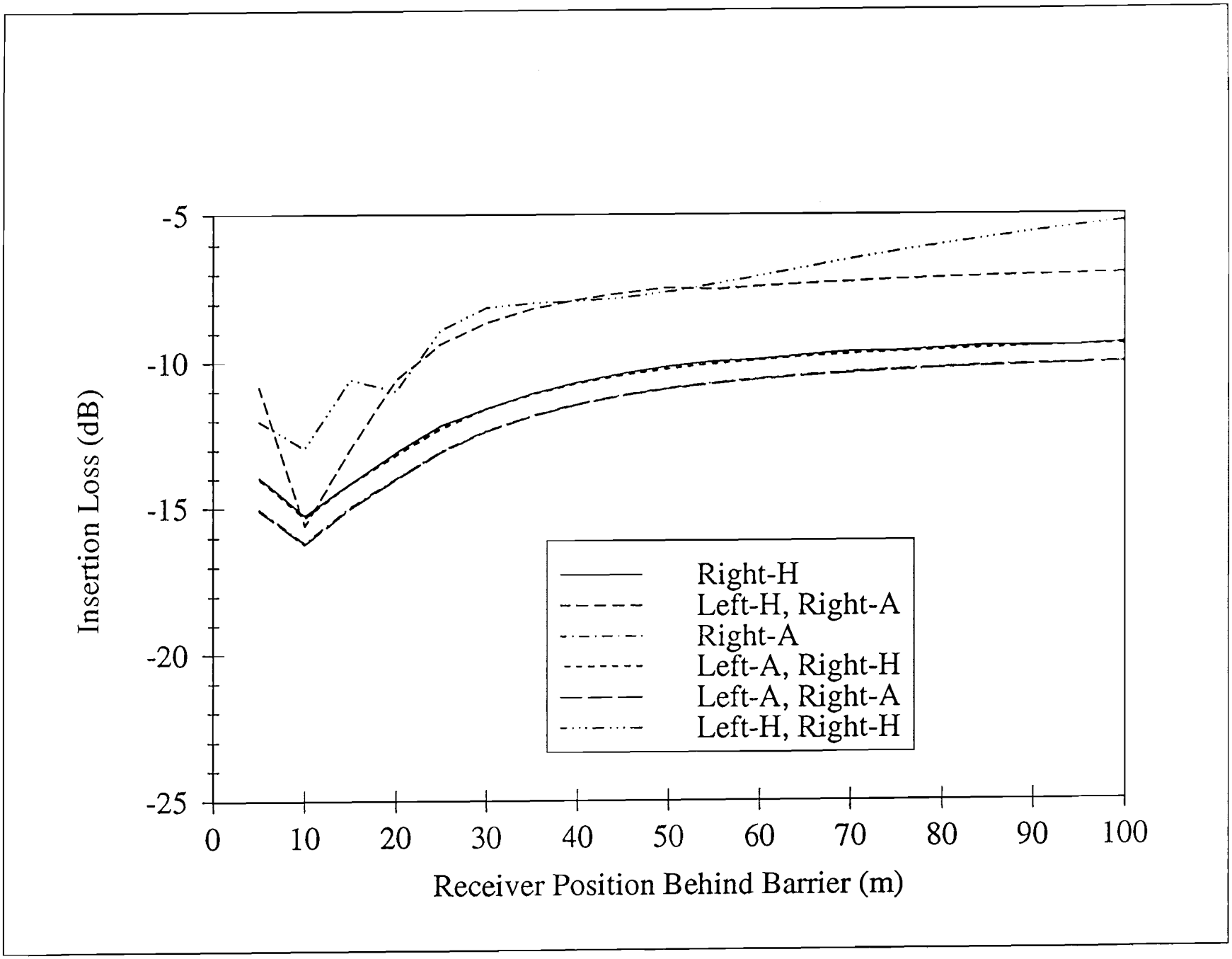

Figure 38 - Single vs. Parallel Barriers

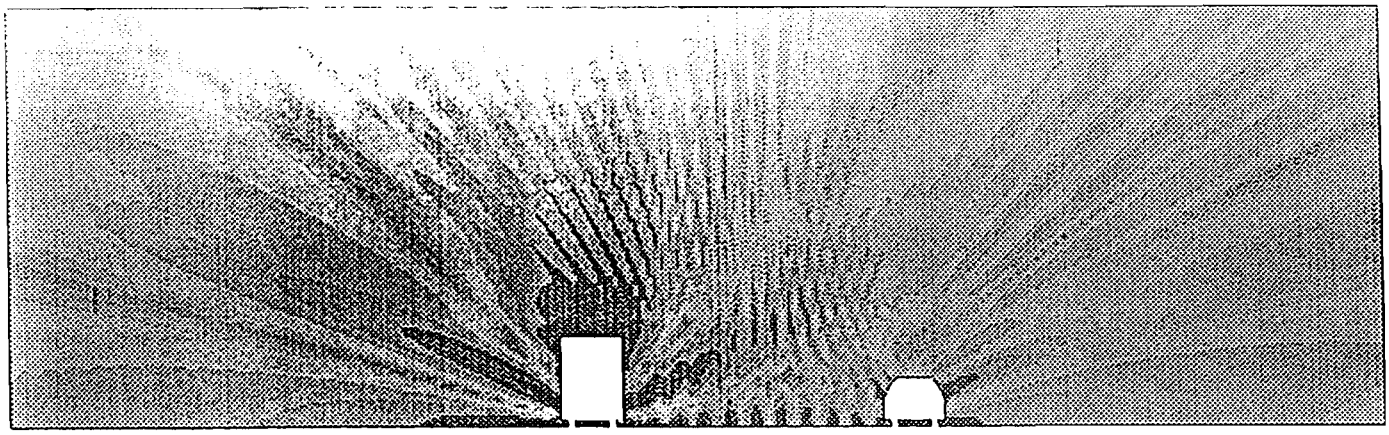

Figure 39 - Complex Geometry #1 - Flat Roadway

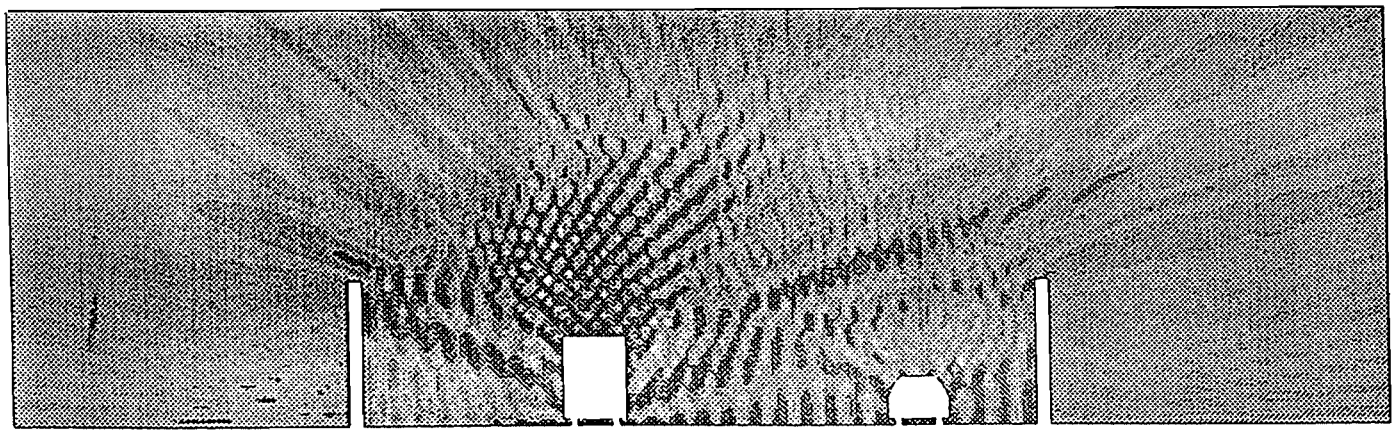

Figure 40 - Complex Geometry #2 - Parallel Barriers on Flat Roadway

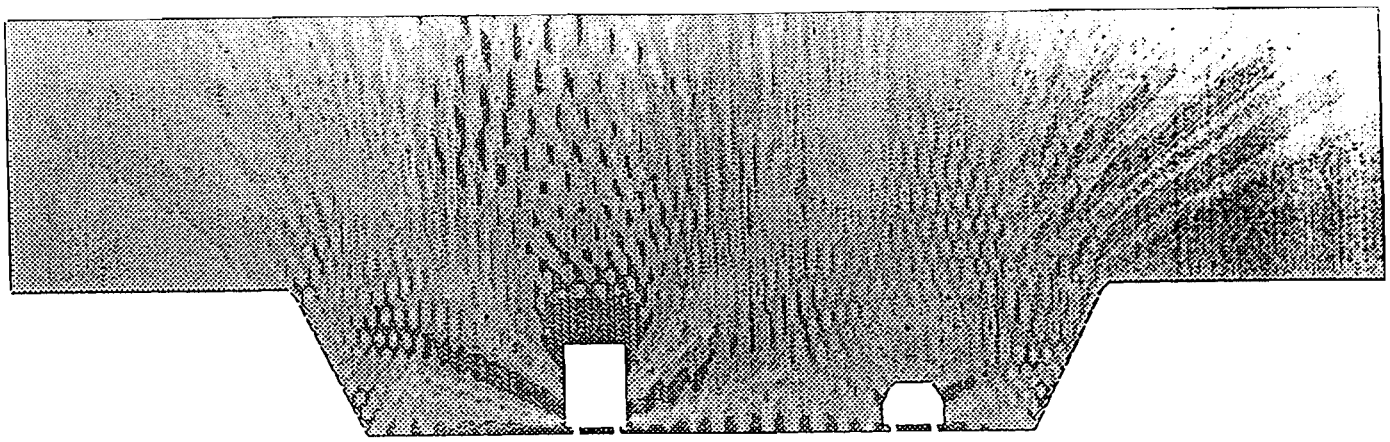

Figure 41 - Complex Geometry #3 - Depressed Roadway

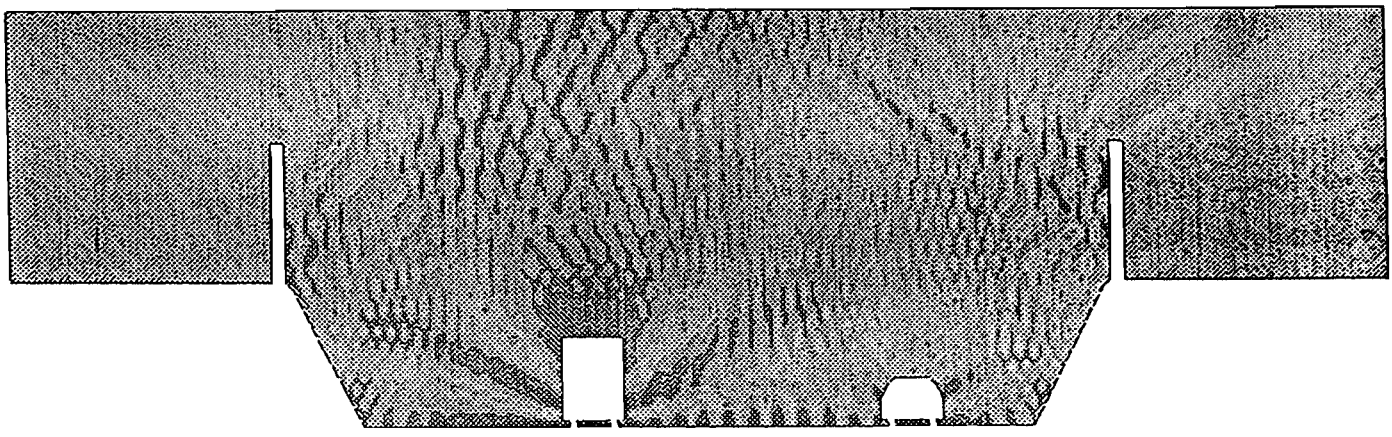

Figure 42 - Complex Geometry #4 - Parallel Barriers on Depressed Roadway

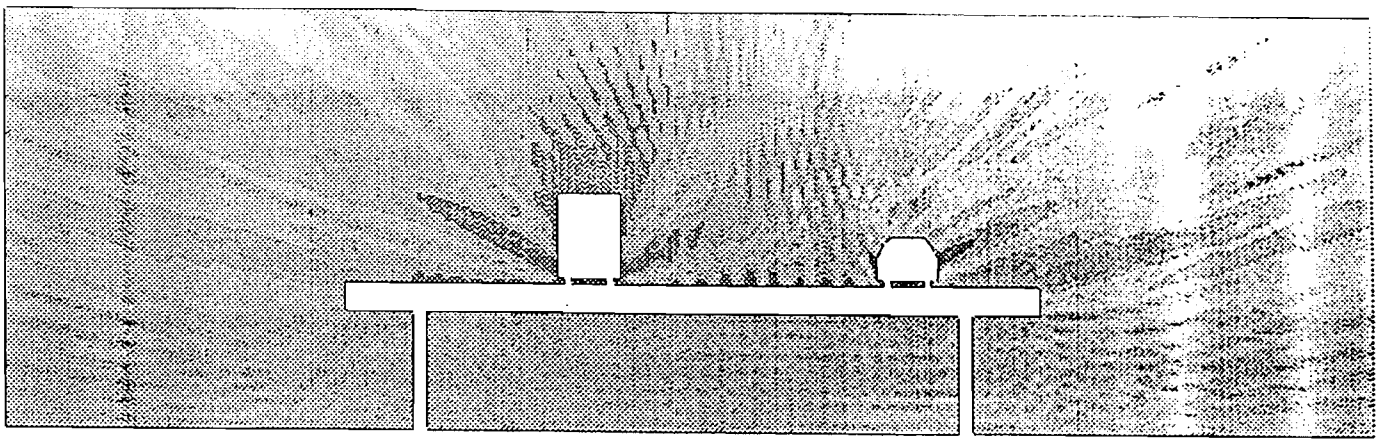

Figure 43 - Complex Geometry #5 - Elevated Roadway

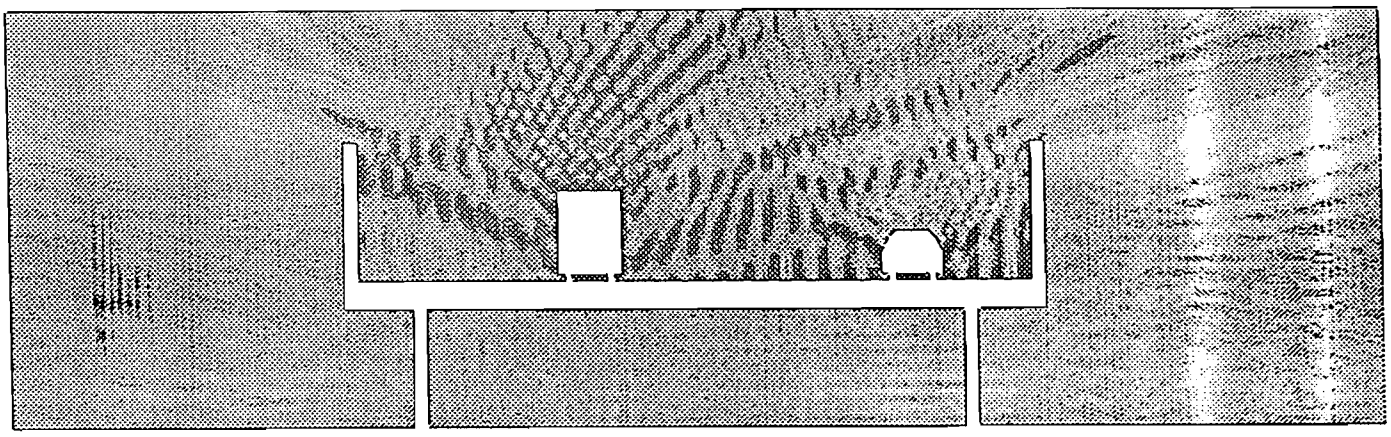

Figure 44 - Complex Geometry #6 - Parallel Barriers on Elevated Roadway

APPENDIX B - THE FRESNEL THEORY OF DIFFRACTION

THE FRESNEL THEORY OF DIFFRACTION

By constructing a wavefront using Huygens' principle, diffraction behaviour can be observed. Huygens' principle states that "every point on a wavefront, as it vibrates, becomes the origin of secondary waves, which diverge in spheres, so that the wavefront at a succeeding incident is the envelope of these secondary waves. The disturbance is not propagated back to the origin because of the principle of interference, by Kirchoff, that the effects of secondary waves mutually destroy each other around the envelope, so that the wave is propagated only in the direction away from the origin" [37]. A diffracted ray is formed after an incident ray contacts a surface, for example the tip of a barrier.

The Fresnel theory of diffraction [10] makes its foundation on "half-period" zones. Consider a point source S. A perpendicular path from a wavefront to a receiver R represents the shortest possible path 'b' from the wavefront to R. Subsequent paths, each ½λ longer than 'b', can then be drawn from R to the wavefront, as in Figure B1. The path length, from S, to the point where a path 'b + λ/2' intersects the wavefront, to R, exceeds the direct path length from H to P by ½λ. This is the origin of the term path length difference:

$$\delta = a + b - d$$

The path length difference can be considered positive on the upper half of the wavefront and negative on the lower half. This series of paths will form circles on the wavefront. A "half-period" zone consists of the area of one ring formed by these circles, denoted by S_1, S_2, etc in Figure B2. The ellipse through the source, the receiver and the wavefront intersection can be defined as a Fresnel zone [38]. The Fresnel number can now be defined as the zone number or the number of half-wavelengths of path length difference:

$$N = \frac{2\delta}{\lambda}$$

Due to the convention of path length difference, there exist both positive and negative Fresnel zone numbers. The "half-period" zones constructed on the wavefront are of approximately equal area. Each secondary path, or wavelet, travels a path to R that differs by ½λ and thus each path reaches R with a maximum phase shift of π. Then, if successive zone amplitudes are added, the resultant amplitude at R can be obtained. Fresnel postulated that the amplitude of successive zones decreased and in summation, that the resultant amplitude at R was either half the sum or half the difference of the contributions from the first and last zones. If the entire field were considered, the last zone amplitude would approach zero and the resultant amplitude at R would be half that of the first zone. The zones could be divided further, creating sub-zones, resulting in contributions of different phases and amplitudes at R. Fresnel's vibration spiral, Figure B3, was then formed to describe this phenomena.

Now consider a cylindrical, or line, source. Strips, instead of circles are now formed on the wavefront using the same procedure as above, as in Figure B4. The area of each strip is no longer equal as the area proportional to the width of the strip. Thus, the amplitude contribution, from each zone decreases more rapidly. The amplitude diagram in Figure B5 formed is now Cornu's spiral, a case specific version of the vibration spiral. The curve is characterized by the distance along the curve from the origin, v and the angle delta representing the phase lag. Fresnel's integrals attempt to describe this spiral in x and y coordinates.

For a traffic noise application, the barrier would be considered as a straight edge in between the source S and receiver P, with the wavefront placed at the barrier, similar to that in Figure B6. The first and last "half-period" zone of the wavefront that is not shielded from the receiver must be plotted on the spiral. The resultant amplitude and phase at P would then obtained by joining these two points [10]. According, then to Cornu's spiral, the amplitude and phase of the sound plane wave can vary from point to point [15] thus suggesting an optimum location for the receiver or barrier.

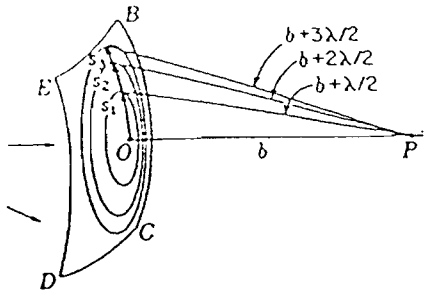

Figure B1 - Fresnel Zones for Point Source

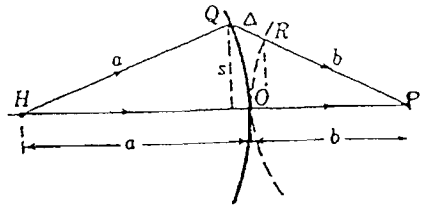

Figure B2 - Path Length Difference

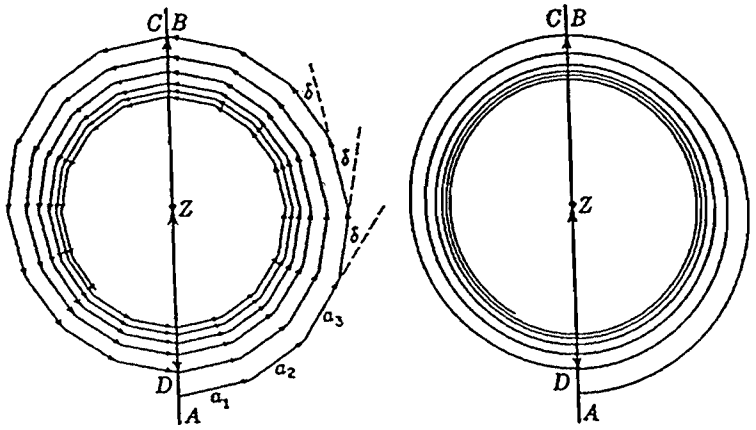

Figure B3 - Fresnel Vibration Spiral

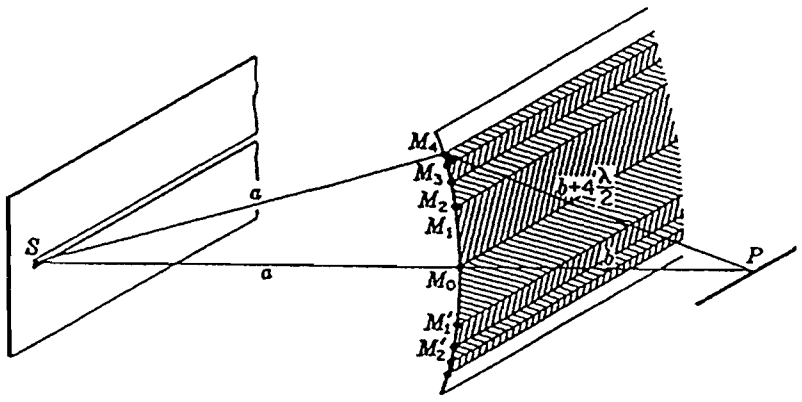

Figure B4 - Fresnel Zones for Cylindrical Source

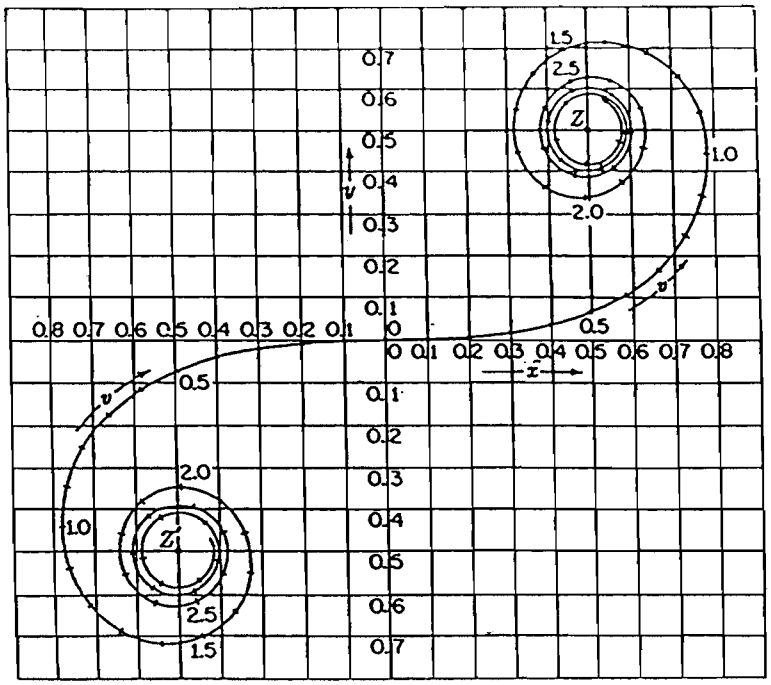

Figure B5 - Cornu's Spiral

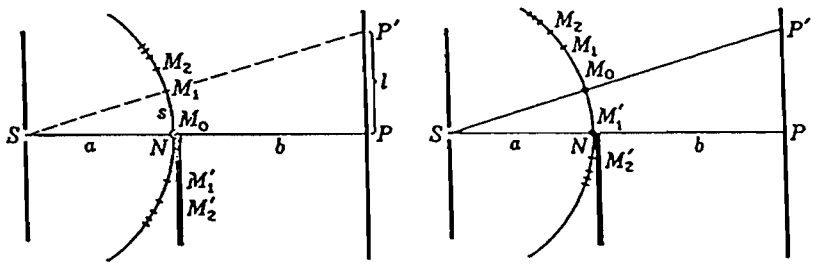

Figure B6 - Fresnel Diffraction

APPENDIX C - CMHC TABLES

Ratio v/g	Ratio u/g														
	over 9.5	8.6 to 9.5	7.6 to 8.5	6.6 to 7.5	5.6 to 6.5	4.6 to 5.5	3.6 to 4.5	2.8 to 3.5	2.3 to 2.7	1.8 to 2.2	1.3 to 1.7	0.9 to 1.2	0.6 to 0.8	0.36 to 0.50	0.15 to 0.35	less than 0.15
over 9.5	10.0	9.0	9.0	8.0	7.0	6.0	5.0	4.0	4.0	3.0	2.0	1.5	1.0	1.0	0.7	0.7
8.6 - 9.5	9.0	9.0	8.0	7.0	7.0	6.0	5.0	4.0	4.0	3.0	2.0	1.5	1.0	1.0	0.7	0.7
7.6 - 8.5	9.0	8.0	8.0	7.0	7.0	6.0	5.0	4.0	4.0	3.0	2.0	1.5	1.0	1.0	0.7	0.7
6.6 - 7.5	8.0	7.0	7.0	7.0	6.0	6.0	5.0	4.0	3.0	3.0	2.0	1.5	1.0	1.0	0.7	0.7
5.6 - 6.5	7.0	7.0	7.0	6.0	6.0	5.0	5.0	4.0	3.0	3.0	2.0	1.5	1.0	1.0	0.7	0.7
4.6 - 5.5	6.0	6.0	6.0	6.0	5.0	5.0	4.0	4.0	3.0	3.0	2.0	1.5	1.0	1.0	0.7	0.7
3.6 - 4.5	5.0	5.0	5.0	5.0	5.0	4.0	4.0	3.0	3.0	2.5	2.0	1.5	1.0	1.0	0.7	0.7
2.8 - 3.5	4.0	4.0	4.0	4.0	4.0	4.0	3.0	3.0	2.5	2.5	2.0	1.5	1.0	1.0	0.7	0.7
2.3 - 2.7	4.0	4.0	4.0	4.0	4.0	3.0	3.0	2.5	2.5	2.0	2.0	1.5	1.0	1.0	0.7	0.7
1.8 - 2.2	3.0	3.0	3.0	3.0	3.0	3.0	2.5	2.5	2.0	2.0	1.5	1.5	1.0	1.0	0.7	0.7
1.3 - 1.7	2.0	2.0	2.0	2.0	2.0	2.0	2.0	2.0	2.0	1.5	1.5	1.0	1.0	1.0	0.7	0.7
0.9 - 1.2	1.5	1.5	1.5	1.5	1.5	1.5	1.5	1.5	1.5	1.5	1.0	1.0	0.7	0.7	0.7	0.5
0.6 - 0.8	1.0	1.0	1.0	1.0	1.0	1.0	1.0	1.0	1.0	1.0	1.0	0.7	0.7	0.5	0.5	0.3
0.36- 0.5	1.0	1.0	1.0	1.0	1.0	1.0	1.0	1.0	1.0	1.0	1.0	0.7	0.5	0.5	0.3	0.0
0.15- 0.35	0.7	0.7	0.7	0.7	0.7	0.7	0.7	0.7	0.7	0.7	0.7	0.7	0.5	0.3	0.3	0.0
less than 0.15	0.7	0.7	0.7	0.7	0.7	0.7	0.7	0.7	0.7	0.7	0.7	0.5	0.3	0.0	0.0	0.0

Table C1 - CHMC Effective Barrier Length Ratio

Path Length Difference (in metres)		Effective Barrier Length Ratio (w) 0.3	0.5	0.7	1.0	1.5	2.0	2.5	3.0	4.0	5.0	6.0	7.0	8.0	9.0	10.0	Infinite Length
		Barrier Attenuation (in dB)															
barrier does not interrupt line of sight	0.06	0	0	0	0	0	0	0	0	0	0	0	0	0	0	0	0
	0.05	0	0	1	1	1	1	1	1	1	1	1	1	1	1	1	1
	0.04	1	1	2	2	2	2	2	2	2	2	2	2	2	2	2	2
	0.03	1	2	2	2	3	3	3	3	3	3	3	3	3	3	3	3
	0.02	1	2	2	3	4	4	4	4	4	4	4	4	4	4	4	4
	0.00	1	2	2	3	4	5	5	5	5	5	5	5	5	5	5	5
barrier does interrupt line of sight	0.03	1	2	3	4	5	6	6	6	6	6	6	6	6	6	6	6
	0.07	1	2	3	4	5	6	6	6	7	7	7	7	7	7	7	7
	0.13	1	2	3	4	6	7	7	7	8	8	8	8	8	8	8	8
	0.20	1	2	3	4	6	7	7	8	9	9	9	9	9	9	9	9
	0.30	1	2	3	4	6	7	8	9	9	10	10	10	10	10	10	10
	0.41	1	2	3	4	6	7	8	9	10	10	11	11	11	11	11	11
	0.55	1	2	3	4	6	8	9	10	11	11	12	12	12	12	12	12
	0.79	1	2	3	4	6	8	9	10	11	11	12	12	12	12	12	13
	1.0	1	2	3	4	6	8	9	10	11	12	12	13	13	13	13	14
	1.4	1	2	3	4	6	8	9	10	11	12	12	13	14	14	14	15
	1.8	1	2	3	4	6	8	9	10	12	13	13	14	14	14	15	16
	2.5	1	2	3	4	6	8	9	10	12	13	14	15	15	15	16	17
	3.3	1	2	3	4	6	8	9	11	12	13	15	15	16	16	17	18
	4.5	1	2	3	4	6	8	9	11	12	14	15	16	17	17	18	19
	6.0	2	3	3	5	7	8	10	11	13	15	16	17	18	18	19	20

Table C2 - CHMC Barrier Attenuation

Effective Total Height Above Ground (metres)	HORIZONTAL DISTANCE FROM SOURCE TO RECEIVING POINT (METRES)																	
	up to 11	11 to 14	15 to 18	19 to 22	23 to 27	28 to 35	36 to 45	46 to 57	58 to 72	73 to 90	91 to 112	113 to 142	143 to 180	181 to 225	226 to 275	276 to 350	351 to 450	451 or over
	Correction in dB if acoustically "soft" surface																	
58.0 or over	+5	+4	+3	+2	+1	0	-1	-2	-3	-4	-5	-6	-7	-8	-9	-11	-13	-15
45.1 to 57.0	+5	+4	+3	+2	+1	0	-1	-2	-3	-4	-5	-6	-7	-8	-10	-12	-14	-16
36.1 to 45.0	+5	+4	+3	+2	+1	0	-1	-2	-3	-4	-5	-6	-7	-9	-11	-13	-15	-17
28.1 to 36.0	+5	+4	+3	+2	+1	0	-1	-2	-3	-4	-5	-6	-8	-10	-12	-14	-16	-18
22.1 to 28.0	+5	+4	+3	+2	+1	0	-1	-2	-3	-4	-5	-7	-9	-11	-13	-15	-17	-19
18.1 to 22.0	+5	+4	+3	+2	+1	0	-1	-2	-3	-4	-6	-8	-10	-12	-14	-16	-18	-20
14.1 to 18.0	+5	+4	+3	+2	+1	0	-1	-2	-3	-5	-7	-9	-11	-13	-15	-17	-18	-20
11.1 to 14.0	+5	+4	+3	+2	+1	0	-1	-2	-4	-6	-8	-10	-12	-14	-16	-17	-19	-21
9.1 to 11.0	+5	+4	+3	+2	+1	0	-1	-3	-5	-7	-9	-11	-13	-15	-17	-18	-20	-21
7.1 to 9.0	+5	+4	+3	+2	+1	0	-2	-4	-6	-8	-10	-12	-14	-16	-17	-19	-20	-22
5.6 to 7.0	+5	+4	+3	+2	+1	-1	-3	-5	-7	-9	-11	-13	-14	-16	-18	-19	-20	-22
4.1 to 5.5	+5	+4	+3	+2	0	-2	-4	-6	-8	-10	-12	-14	-15	-17	-18	-20	-21	-23
2.6 to 4.0	+5	+4	+3	+1	0	-2	-4	-6	-8	-10	-12	-14	-16	-18	-19	-21	-22	-24
up to 2.5	+5	+4	+3	+1	-1	-3	-5	-7	-9	-11	-13	-15	-17	-19	-21	-22	-23	-25
	Correction in dB if acoustically "hard" surface																	
All Heights	+5	+4	+3	+2	+1	0	-1	-2	-3	-4	-5	-6	-7	-8	-9	-10	-11	-12

Table C3 - CHMC Distance Correction

APPENDIX D - CROWN TABLES

	Shadow zone	*Illuminated zone*
A_0	−15.4	0
A_1	−8.26	+0.109
A_2	−2.787	−0.815
A_3	−0.831	+0.479
A_4	−0.198	+0.3284
A_5	+0.1539	+0.04385
A_6	+0.12248	
A_7	+0.02175	
Range of validity	$-3 \leq x \leq +1.2$	$-4 \leq x \leq 0$

Table D1 - Crown Polynomials

Shadow zone	*Illuminated zone*
For $x < -3$ $A = -5.0$ For $x > 1.2$ $A = -30$	For $x < -4$ $A = -5.0$ For $x > 0$ $A = 0$

Table D2 - Crown Alternate Ranges

APPENDIX E - ABSORPTIVE COATINGS

ABSORPTIVE COATINGS

Except where indicated otherwise, the absorbent material applied to all surfaces in this study has an absorption coefficient of 1.00, converting to a specific impedance of 1.00, and a normal impedance of 416.5, with ρ=1.225 kg/m^3 and 340 m/s. This is the maximum theoretical absorption possible. By assessing absorptive barriers solely at this level, the maximum theoretical performance can be measured. However, typical materials will not perform at this level. Instead, typical materials will perform in the range between the extremes of the perfectly hard and the perfectly absorbing cases.

Table E1 - Parameters to Describe Varying Surface Treatments

Absorption Coefficient, α	Flow (MKS) Resistance, σ	Impedance	Admittance
0.00	∞	∞	0
0.10	1945000	35400	2.82E-05
0.20	577000	14500	6.90E-05
0.30	268000	8330	1.20E-04
0.40	200000	6660	1.50E-04
0.50	96000	4080	2.45E-04
0.60	58000	2950	3.39E-04
0.70	38000	2200	4.55E-04
0.80	20000	1600	6.25E-04
0.90	10250	1100	9.09E-04
1.00	0	416.5	2.40E-03

Table E1 displays the approximate relationships between the real impedance and real admittance and the absorption coefficient, α, and flow resistance, σ. The impedance is defined using the empirical relations by Kuttruff [39] for absorption coefficient,

$$\alpha = 8\xi[1 + \frac{\xi^2 + \sigma^2}{\sigma} \tan^{-1}(\frac{\sigma}{\sigma^2 + \xi^2 + \sigma}) - \xi \ln(\frac{(\xi + 1)^2 + \sigma^2}{\sigma^2 + \xi^2})]$$

where ξ and σ are the real and imaginary components of the specific admittance, and by the Delany and Bazley [40] derivation for flow resistance,

$$Z = 1 + 9.08(\frac{1000f}{\sigma})^{-0.75} + i11.9(\frac{1000f}{\sigma})^{-0.73}$$

where the imaginary component of the impedance, in both cases, is assumed to be zero. Values of α=0.33 and σ=250,000 MKS are typical of grassland surfaces [41] and the values α=0.05 and σ=2,500,000 are representative of brick surfaces [42].

REFERENCES

1) Z. Maekawa, "Noise Reduction by Screens," Applied Acoustics **1**, 57-173 (1968).

2) U.J. Kurze, "Noise Reduction by Barriers," J. Acoust. Soc. Am. **55** (3), 504-518 (1974).

3) De Leuw Cather, "Manual for the Prediction of Surface Transportation Noise and for its Control Through Facility Design," Alberta Transportation. (1975)

4) T.M. Barry and J.A. Reagan, "FHWA Highway Traffic Noise Prediction Model," Fed. Highway Admin., Report No. FHWA-RD-77-108 (1978)

5) Canada Mortgage and Housing Corporation, "Road and Rail Noise: Effects on Housing," Report No. NHA 5156 (1981)

6) Department of Transport Welsh Office, "Calculation of Road Traffic Noise," (1988)

7) International Standard Organization, "Acoustics - Attenuation of Sound During Propagation Outdoors - Part 2: A General Method of Calculation," Report No. ISO/DIS 9613-2 (1992)

8) K.R. Fyfe, J.P.G. Coyette and P.A. van Vooren, "Acoustic and Elasto-Acoustic Analysis using Finite Element and Boundary Element Methods," J. Sound and Vibration **25**, 16-22 (1991).

9) M. Born and E. Wolf, *Principles of Optics*, (Pergamon Press, Oxford, 1970) 4th Edition

10) F.A. Jenkins and H.E. White, *Fundamentals of Optics* (McGraw-Hill, Toronto, 1957) 3rd Edition

11) U.J. Kurze and G.S. Anderson, "Sound Attenuation by Barriers," Applied Acoustics **4**, 35-53 (1971).

12) J.B. Keller, "Geometrical Theory of Diffraction," J. Opt. Soc. Am. **52** (2), 116-130 (1962).

13) L.L. Beranek, *Noise Reduction*, (McGraw-Hill, Toronto, 1960)

14) P.M. Nelson, *Transportation Noise Reference Book* (Butterworth and Co., Toronto, 1987)

15) H.G. Jonasson, "Sound Reduction by Barriers on the Ground," J. Sound Vib. **22**, 113-126 (1972).

16) H.A. Schenck, "Improved Integral Formulation for Acoustic Radiation Problem," J. Acoust. Soc. Am. **44**, 41-58, (1967).

17) A.F. Seybert, B. Soenarko, F.J. Rizzo, and D.J. Shippy, "Application of the BIE Method to Sound Radiation Problems Using and Isoparametric Element," ASME paper #82 - WA/NCA-1 (1982).

18) G.M.L. Gladwell, "A Finite Element Method for Acoustics," *5^{e} Congress International D'Accoustique*, Liege, Belgium, Paper L33, (1965).

19) A. Craggs, "The use of Simple Three-Dimensional Acoustic Finite Elements for Determining the Natural Modes and Frequencies of Complex Shaped Enclosures," J. Acoust. Soc. Am. **23**, 331-339 (1972).

20) R.J. Astley and W. Eversman, "Finite Element Formulations for Acoustical Radiation," J. Sound Vib. **88** (1), 47-64 (1983).

21) V. Schroter and C.Chiu, "Ontario Road Noise Analysis Method for Environment and Transportation," Ontario Environment, Report No. ISBN-7729-6376 (1990)

22) G. Watts, "Acoustic Performance of Traffic Noise Barriers - A State of the Art Review," Department of Transport, 223-250 (1992).

23) W. Bowlby, J. Higgins and J. Reagan, Noise Barrier Cost Reduction Procedure, STAMINA 2.0/OPTIMA User's Manual, Fed. Highway Admin., Report No. FHWA-DP-58-1 (1982)

24) W. Bowlby and L.F. Cohn, "A Model for Insertion Loss Degradation for Parallel Highway Noise Barriers," J. Acoust. Soc. Am. **80** (3), 855-869 (1986)

25) D.C. Hothersall, S.N. Chandler-Wilde and M.N. Hajmirzae, "Effeciency of Single Noise Barriers," J. Sound and Vibration **146** (2), 303-322 (1991)

26) K.R. Fyfe and C.C. Harrison, "Road Noise Modelling: An Initial Look at the Differences Between Ray and Wave-Based Techniques for the Prediction of the Attenuative Effects of a Road Noise Barrier, CMHC External Grant preliminary report, Nov, 1993.

27) ANSYS User's Manual, Version 5.0 Swanson Analysis Systems Inc. Houston, PA 1992

28) SYSNOISE User's Manual, Version 4.4A Numerical Integration Technologies, Leuven Belgium 1992

29) L. Cremers, K.R. Fyfe and J.P. Coyette, "A Variable Order Infinite Acoustic Wave Envelope Element," J. Sound and Vibration, in press, (1993)

30) D.A. Hutchins, H.W. Jones and L.T. Russell, "Model Studies of Barrier Performance in the Presence of Ground Surfaces. Part I - Thin, Perfectly Reflecting Barriers," J. Acoust. Soc. Am. 75 (6), 1807-1816 (1984)

31) P.T. Lewis, The Noise Generated by Single Vehicles in Freely Flowing Traffic. *J. Sound and Vibration*, **30**(2) (1973) 207-220

32) A. Alexandre, J.Ph. Barde, C. Lamure, and F.J. Langdon, Road Traffic Noise (Applied Science Publishers Ltd., London, 1975)

33) D.D. Reynolds, Engineering Principles of Acoustics - Noise and Vibration Control (Allyn and Bacon Inc., Toronto, 1981)

34) D.C. Hothersall, D.H. Crombie and S.N. Chandler-Wilde, The Performance of T-Profile and Associated Noise Barrier. *Applied Acoustics*, **32** (1991) 269-287

35) United States Department of Transportation, Federal Highway Administration, "Highway Traffic Noise Barrier Construction Trends", *The Wall Journal*, **14** (1994) 8-16

36) CSI, "Soundtrap", *The Wall Journal*, **14** (1994) 14

37) F.G. Richardson, *Sound*, (Edward Arnold and Co., London, 1927)

38) J.W. Strutt and Baron Raleigh, *Theory of Sound*, (Macmillan and Co., London, 1896)

39) H. Kuttruff, Room Acoustics, (Applied Science Publishers, London, 1979)

40) M.E. Delany, and E.N. Bazley, Acoustical Properties of Fibrous Absorbent Materials. *Applied Acoustics*, **3** (1970) 357-391

41) K.B. Rasmussen, Sound Propagation Over Grass Covered Ground. *J. Sound and Vibration*, **78**(2) (1981) 247-255

42) K. Attenborough, Acoustical Impedance Models for Outdoor Ground Surfaces. *J. Sound and Vibration*, **99**(4) (1985) 521-544